Journal of Volcanology and Geothermal Research 421 (2022) 107429

Contents lists available at ScienceDirect

Journal of Volcanology and Geothermal Research

journal homepage: www.elsevier.com/locate/jvolgeores

The hazards of unconfined pyroclastic density currents: A new synthesis and classification according to their deposits, dynamics, and thermal and impact characteristics

Geoffrey A. Lerner [a,b,*], Susanna F. Jenkins [a,b], Sylvain J. Charbonnier [c], Jean-Christophe Komorowski [d], Peter J. Baxter [e]

[a] Earth Observatory of Singapore, Nanyang Technological University, 50 Nanyang Avenue, Block N2-01a-15, Singapore 639798, Singapore
[b] Asian School of Environment, Nanyang Technological University, 62 Nanyang Dr, Singapore 637459, Singapore
[c] School of Geosciences, University of South Florida, 4202 E. Fowler Avenue, NES 107, Tampa, FL 33620-5550, USA
[d] Institut de Physique du Globe de Paris, Université de Paris, CNRS, 1, rue Jussieu, Paris 75238 Cedex 05, France
[e] Department of Public Health and Primary Care, Institute of Public Health, University of Cambridge, Forvie Site, Robinson Way, Cambridge CB2 0SR, UK

ARTICLE INFO

Article history:
Received 3 June 2021
Received in revised form 5 November 2021
Accepted 10 November 2021
Available online 16 November 2021

Keywords:
Volcano
Pyroclastic flow
Pyroclastic surge
Merapi
Fuego

ABSTRACT

Pyroclastic density currents (PDCs) that escape their confining channels are among the most dangerous of volcanic hazards. These unconfined PDCs are capable of inundating inhabited areas that may be unprepared for these hazards, resulting in significant loss of life and damage to infrastructure. Despite their ability to cause serious impacts, unconfined PDCs have previously only been described for a limited number of specific case studies. Here, we carry out a broader comparative study that reviews the different types of unconfined PDCs, their deposits, dynamics and impacts, as well as the relationships between each element. Unconfined PDCs exist within a range of concentration, velocity and temperature: characteristics that are important in determining their impact. We define four end-member unconfined PDCs: 1. fast overspill flows, 2. slow overspill flows, 3. high-energy surges, and 4. low-energy detached surges (LEDS), and review characteristics and incidents of each from historical eruptions. These four end-members were all observed within the 2010 eruptive sequence of Merapi, Indonesia. We use this well-studied eruption as a case study, focusing on the villages of Bakalan (13 km south of the volcano) and Bronggang (14 km south of the volcano), which were impacted by slow overspill flows and LEDS, respectively. These two unconfined PDC types are the least described from previous volcanic eruptions, but during the 2010 Merapi eruption the overspill flows resulted in building destruction and the LEDS in significant loss of life. We discuss the dynamics and deposits of these unconfined PDCs, and the resultant impacts. We then use the lessons learned from the 2010 Merapi eruption to assess some of the impacts associated with the deadly 2018 Fuego, Guatemala eruption. Satellite imagery and media images supplementing fieldwork were used to determine the presence of both overspill flows and LEDS, which resulted in the loss of hundreds of lives and the destruction of hundreds of buildings in inundated areas within 9 km of the summit. By cataloguing unconfined PDC characteristics, dynamics and impacts, we aim to highlight the importance and value of accounting for such phenomena in emergency management and planning at active volcanoes.

1. Introduction

Pyroclastic density currents (PDCs) are the deadliest volcanic hazard, accounting for nearly a third of all historical volcano-related fatalities (Brown et al., 2017). They are also some of the most complex and unpredictable volcanic phenomena, which makes accurate forecasting of their occurrence, characteristics and the area impacted difficult. In particular, the ability for PDCs to surmount topography and travel outside of the channels in which they are typically contained can place them in direct contact with communities on the flanks of volcanoes. They can destroy whole towns and kill tens of thousands of people (e.g., St Pierre, Martinique, 1902: Lacroix, 1904), but little is known about their internal dynamic processes, and the ability to measure their dynamics in real time during eruptions does not yet exist. As a result, they pose a significant challenge for emergency management and planning at explosive volcanoes in densely populated regions.

* Corresponding author at: Earth Observatory of Singapore, Nanyang Technological University, 50 Nanyang Avenue, Block N2-01a-15, Singapore 639798, Singapore.
E-mail addresses: geoffrey.lerner@ntu.edu.sg (G.A. Lerner), susanna.jenkins@ntu.edu.sg (S.F. Jenkins), sylvain@usf.edu (S.J. Charbonnier), komorow@ipgp.fr (J.-C. Komorowski), pjb21@medschl.cam.ac.uk (P.J. Baxter).

https://doi.org/10.1016/j.jvolgeores.2021.107429

PDCs are gravity-driven mixtures of hot gases and fragmented volcanic particles (ranging in size from ash through lapilli to blocks and boulders). The term PDC encompasses a wide spectrum of densities and generation mechanisms, within which lie the two end-members of pyroclastic flow (dense, high particle concentration) and surge (dilute, low particle concentration) (Cole et al., 2015). A single PDC is commonly composed of two distinct layers - the denser, gravity driven basal "flow" layer and a more dilute, buoyant upper "surge" layer (Fisher 1995). While these layers can flow in unison under certain conditions (e.g., coupled PDCs in the 2015 eruption at Colima, Mexico; Breard and Lube, 2017; Pensa et al., 2019), it is possible for them to behave independently of each other, with the upper and lower layers moving at different speeds and having different characteristics (Fisher, 1995; Cole et al., 2015). The dense basal layer of a PDC (the flow) is topographically constrained so that its path typically remains confined to within a pre-existing channel, while the dilute, upper layer of PDCs (the surge) is less topographically constrained. Models of PDC transport regimes are improving in their sophistication, with the newest conceptual models including an intermediate flow layer between the dense basal and upper dilute layers (Lube et al., 2020). From a hazards perspective, the difference in characteristics between layers of the PDC is extremely important, as it means the dilute, upper layer can detach from the lower, gravity driven flow, climbing topographic barriers and travelling to places that the rest of the PDC cannot (e.g., Nakada and Fujii, 1993; Loughlin et al., 2002a, 2002b; Dufek et al., 2015; Jenkins et al., 2016). As a result, surges can unexpectedly inundate built areas outside of pre-existing channels, where people are present.

Here we present new detailed data connecting the geology and dynamics of the distal (>10 km) 5 November 2010 unconfined PDCs at Merapi, focussing on their deposit characteristics, generation mechanisms and impacts to buildings, vegetation and victims, who were caught in the process of evacuating. We then use lessons drawn from the analysis of the Merapi 2010 eruption to assess PDC dynamics and impacts from the deadly June 2018 eruption of Volcán de Fuego in Guatemala. Using the same techniques as for Merapi 2010, we use satellite and media images to investigate loss of life and damage to structures caused by unconfined PDCs, supplemented by field studies focused on the deposits, and infer their types and dynamics. Data from both these eruptions provide an empirical foundation for better understanding and forecasting the impacts of unconfined PDCs on communities, highlighting the importance of accounting for the potential for such PDCs in emergency management and planning, even where geological evidence of the PDCs is not preserved.

1.1. Unconfined PDCs

Many recorded volcanic tragedies in the past two centuries have resulted from surges that detached from their parent flows and inundated populated areas (e.g., Unzen 1991, Nakada and Fujii, 1993; Soufrière Hills 1997, Loughlin et al., 2002b; Merapi 2010, Jenkins et al., 2016). While the upper more buoyant surge layer is more likely to be unconfined by channel topography, and thus able to inundate a wider range of areas than the dense basal layer (e.g., Abdurachman et al., 2000; Jenkins et al., 2016), dense flows can also become unconfined during their propagation (e.g., Gertisser et al., 2012; Charbonnier et al., 2013). Such 'unconfining' of the flow and/or surge typically results from a change in the underlying syn-eruptive topography or by an increase of the local mass flux, volume or velocity of the dense flow, which can act to reduce channel capacity or redirect the flow away from the primary channel direction (Lube et al., 2011; Ogburn et al., 2014). These topographic changes can be natural or the result of human intervention, and can cause a PDC to become unconfined in the following ways:

1. *Lateral channel constriction:* Narrowing of the channel in which a PDC is confined reduces the cross-sectional area available and may cause PDCs to expand vertically, making it easier for the PDC to escape the channel (e.g., Merapi 1994 and 2006; Abdurachman et al., 2000; Gertisser et al., 2012). Such constrictions can be the result of natural topographic changes (through erosion and deposition) or concrete channel confinement for lahars (e.g., sabo dams);
2. *Vertical channel constriction:* Shallowing of a channel or prior infilling by deposits will similarly have the effect of reducing the volumetric capacity of the channel and thus promoting the overspill of confined PDCs. Sediment retention dams intended to constrain the flow of lahars can promote this (e.g., Merapi 2010; Charbonnier et al., 2013; Jenkins et al., 2013);
3. *Channel bends or obstructions:* Sudden changes in the direction of the confined flow path of a PDC can promote flow overspill or surge detachment, especially in combination with any of the above factors, as the PDC retains straight-line momentum (e.g., Soufrière Hills, June 1997; Loughlin et al., 2002b);
4. *Slope changes:* Sudden breaks in slope within the channel in which a confined PDC is traveling can cause the decoupling of the upper dilute layer, leading to detachment and overspill (e.g., Ngauruhoe 1975, Nairn and Self, 1978).
5. *Directed eruption:* Eruptions that begin from an explosive eruption that projects energy laterally, rather than as a result of dome or column collapse into channels, will often cause the ensuing PDCs to be unconfined from their point of inception (e.g., Mt. St. Helens 1980; Lipman and Mullineaux, 1982; Belousov et al., 2007).

PDC overspill and detachment are more likely when a channel is near capacity, for example through previous infilling from confined PDCs, which reduces the height difference between valley base and top (Lube et al., 2011; Charbonnier et al., 2013). This can be exacerbated by the pulsating behaviour of PDCs in some eruptions, in which flows from repeated pulses of eruption can progressively infill the channel (Sulpizio and Dellino, 2008; Charbonnier and Gertisser, 2011). Unsteady flow conditions and increases in flow characteristics such as velocity, thickness, and volume may promote overspilling (Charbonnier et al., 2013).

1.2. PDC impacts

The damage to communities caused by unconfined PDCs varies as a function of the PDC concentration, velocity, temperature, as well as other characteristics such as the transport of large clasts and debris that can act as missiles (Pittari et al., 2006; Cole et al., 2015). For example, flow overspill typically causes impact through a combination of dynamic pressure, burial under metres of deposit, and/or thermal impact from temperatures that can reach over 800 °C (Cole et al., 2015), with near binary loss of life or infrastructure. By contrast, surge detachment can cause little physical damage because of low dynamic pressures and very thin (centimetres) remaining deposits, but their thermal impact can still cause casualties and indirect damage through fire (e.g., Baxter et al., 2005; Jenkins et al., 2013; Baxter et al., 2017). The dynamic characteristics of unconfined PDCs, and therefore the type and severity of impacts sustained, vary greatly depending on the generation mechanism and travel path of the PDC, as well as the mechanism through which overspill or detachment occurs. As a result, forecasting the occurrence and impacts associated with unconfined PDCs, across time and space, remains very challenging. Data for better understanding, and therefore forecasting, such events typically arise from field data, numerical modelling (e.g., Valentine and Wohletz, 1989; Neri et al., 2003; Esposti Ongaro et al., 2012; Benage et al., 2016) and/or large-scale experiments (e.g., Dellino et al., 2010; Lube et al., 2015; Brosch and Lube, 2020). Here, we focus on the value of the first: empirical observations and measurements, and how they can be supplemented with remote observations.

Despite their ability to cause serious impacts, unconfined PDCs have been previously described on a limited number of occasions, often tied to specific case studies in notable eruption sequences

(e.g., Abdurachman et al., 2000; Loughlin et al., 2002b; Charbonnier and Gertisser, 2008; Macorps et al., 2018). The lack of a broader comparative study of the different types of unconfined PDCs, and the relationships between their occurrence, deposits, dynamics and the impacts they cause, leaves a gap in the literature that we aim to fill with this study. We review the physical characteristics and devastating impacts associated with unconfined PDCs and provide new geological, impact and casualty data on a subset of these unconfined PDCs – slow overspill flows and low-energy detached surges during the Merapi 2010 eruption, Indonesia. We focus on these two types of unconfined PDC as their impacts are not necessarily binary, i.e. buildings, infrastructure and vegetation may be damaged but not destroyed, and probabilities of survival or escape may be higher than for the higher-energy flows and surges. Low-energy, detached surges have been well-documented in only two previous cases: the 1997 eruption of Soufrière Hills Volcano, Montserrat (Loughlin et al., 2002a, 2002b), and the 1994 eruption of Merapi, Indonesia (Abdurachman et al., 2000; Voight et al., 2000). The Merapi 2010 eruption provides a particularly relevant case study as it involved a wide variety of unconfined PDC types over the course of its eruptive sequence (Charbonnier et al., 2013; Cronin et al., 2013; Komorowski et al., 2013; Jenkins et al., 2016). This included significant impacts related to low-energy detached surges for which deposits were only centimetres thick and therefore unlikely to be preserved in the geological record. The events involving such detached surges and channel overspill flows during the 2010 Merapi eruption are summarised in Komorowski et al. (2013), Cronin et al. (2013), Charbonnier et al. (2013), Jenkins et al. (2013, 2016), and Baxter et al. (2017).

2. Types of unconfined PDCs

Unconfined PDCs can be categorized by two main characteristics: their concentration and their velocity (Fig. 1). The full spectrum of unconfined PDCs can be plotted within this matrix, with the following four end-member types as follows:

- **Fast overspill flows (high-velocity/high-concentration)** – spillout that occurs when a fast-moving, dense, channel-confined PDC is no longer constrained by a channel and invades adjacent areas;
- **Slow overspill flows (low-velocity/high-concentration)** – a dense, unconfined PDC that is moving at low speed, including the margin of a dense unconfined PDC that has slowed considerably from the speed of its confined parent flow;
- **High-energy surges (high-velocity/low-concentration)** – a dilute, directed PDC often stemming from a dome explosion that is typically unconfined from its inception;
- **Low-energy detached surges (low-velocity/low-concentration)** – the dilute, upper portion of a PDC that has decoupled from its denser basal parent flow, allowing it to travel to and invade areas not reached by the denser flows.

Characteristics associated with key types of unconfined PDCs are outlined in Fig. 1, which highlights the wide range of impacts and deposits that can be produced; we provide more discussion and case studies below. Velocity and concentration thresholds are not easy to define

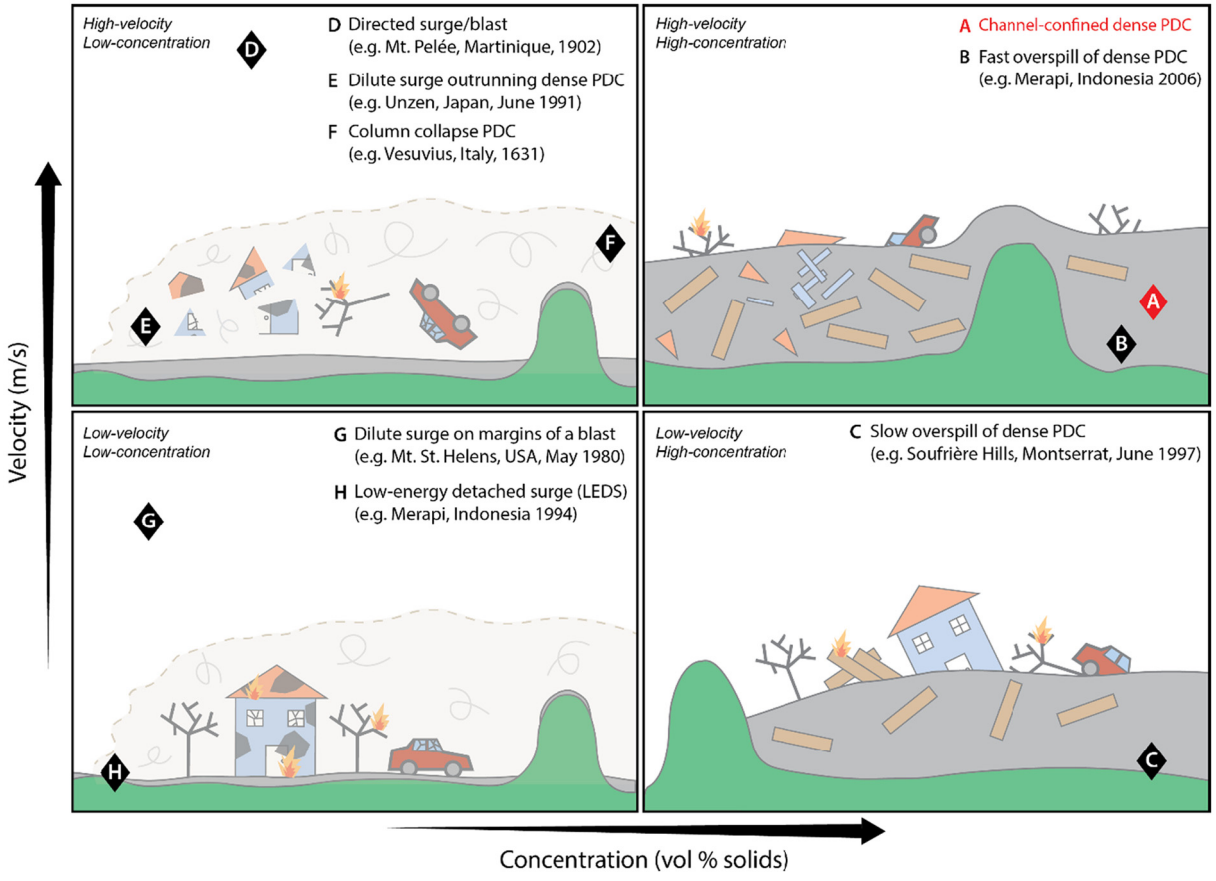

Fig. 1. Unconfined Pyroclastic Density Current (PDC) matrix with schematics showing the interaction between PDC and topography, some impacts and an indication of the remaining deposit associated with the four end-member unconfined PDCs. Black diamonds indicate the relative velocity and concentration of the different types of unconfined PDCs, with one historical example shown for each type. The red diamond represents the characteristics of a high-energy channel-confined PDC for comparison. Note: Many of the eruptions provided as examples for each particular PDC type contained other PDC types as well. Citations for each eruption as follows: B) Gertisser et al. (2012), C) Loughlin et al. (2002b), D) Anderson and Flett (1902), E) Nakada and Fujii (1993), F) Rosi et al. (1993), G) Lipman and Mullineaux (1982), H) Abdurachman et al. (2000).

but approximate thresholds can be based on dynamics inferred or recorded in previous PDCs. We apply thresholds of 5 m/s for velocity and 1% depth-averaged solid particle concentration by volume of the lower 5–10 m of the current as indicative values for the boundary between "high" and "low" (Cole et al., 2015, Dufek et al. 2015) (Fig. 1).

2.1. Fast overspill flows

Fast overspill flows represent the high-velocity, high-concentration end-member of the unconfined PDC matrix (Fig. 1, top right). These flows are closely related to their parent channel-confined PDCs, and typically occur when the mass/volumetric flux of PDC in a channel surpasses the space available in the channel to contain it; for example through channel infilling from previous deposits (Newhall et al., 2000; Charbonnier and Gertisser, 2008). The result is the flow extending laterally beyond the banks of its confining channel and inundating areas adjacent to the channel (e.g., Merapi 2006, Gertisser et al., 2012). This can also occur at bends in a channel where the straight-line momentum of the PDC is sufficient to overtop the topographic margins of the channel (e.g., Varner et al., 2019; Albino et al., 2020). As a result, overspill flows are typically close to the velocity of their parent channel-confined flows, which typically travel at speeds of up to 30 m/s and occasionally up to 60 m/s (Cole et al., 2015).

Overspill PDCs maintain both their high temperature and dynamic pressure, and thus cause damage through both heat and force. Parent channel-confined flows from hot lava dome collapse can be over 600 °C, and fast overspills have been determined in several occurrences to have temperatures at or near their parent flows (e.g., Wibowo et al., 2018), which can have dynamic pressures over 100 kPa near source and over 15 kPa in distal areas (Macorps et al., 2018). As with channel-confined PDCs, overspill flows typically destroy everything in their path, and cause the death and burial of people in inundated areas. For example, overspill flows during the 2006 eruption of Merapi caused two deaths through burial and destroyed several buildings in the village of Kaliadem, ~5 km from the volcano (Gertisser et al., 2012). Similar impacts are sustained by vegetation and infrastructure, with the high dynamic pressures damaging, bending, or completely knocking down trees and utility poles (e.g., Merapi 1994; Abdurachman et al., 2000).

Since these overspill flows represent only the portion of the flow capable of extending beyond the channel, the deposits can be thin relative to the channel-confined PDC, but still geologically significant, on the order of 10s of centimetres to metres thick. Overspill deposits in the 2010 Merapi eruption were typically ~1–2 m thick, and in isolated locations up to 5 m thick (Cronin et al., 2013), significantly thinner than the metres-thick channelized deposits, but thicker than the centimetres thick surge deposits (Charbonnier et al., 2013; Komorowski et al., 2013). Fast overspill flow deposits are typically poorly sorted and can contain up to metre-sized blocks in a medium or fine-grained ash matrix and are often not significantly visually distinct from confined flow deposits other than a generally lower presence of large clasts (Charbonnier and Gertisser, 2008; Gertisser et al., 2012).

2.2. Slow overspill flows

Low-velocity, high-concentration PDCs are frequently represented by the peripheral edges or front of a slowing flow but can also happen when a slow-moving dense flow escapes the bounds of its channel (Fig. 1, bottom right). As flows (channel-confined or not) reach areas more distal from the volcano or branches of the flow move farther from the primary flow axis, they reduce in energy (and therefore velocity) as a result of basal drag or friction acting on the dense layer while maintaining the same concentration (Shimizu et al., 2019). The result is a slow moving, but still highly-concentrated PDC. Whereas high pore pressure helps channel-confined PDCs remain mobile due to high thickness, slow, dense overspill flows are less mobile typically because they are thinner than their channelled counterparts and made of highly frictional material (Breard et al., 2019). These dense slow-moving flows are easily stopped by topographic barriers, which the less dense surge portions of the PDC are capable of decoupling from and surpassing (e.g., Soufrière Hills, Loughlin et al., 2002a, 2002b). The fronts of slowing flows can have velocities that have dropped to 1–2 m/s (Cole et al., 2015).

The high-concentration and typically high temperatures (similar to or slightly cooler than their parent fast overspill flows, Trolese et al., 2018) of these flows means that they are still mostly fatal for victims caught within their path; however, impacts on the built environment can be less binary. The lower energy and dynamic pressures associated with a slower moving flow leads to inundation or damage of buildings and other infrastructure, with the peripheral parts of flows sometimes moving into or around impacted structures rather than sweeping them away (as described in Section 3.3; e.g., Merapi 2006, Gertisser et al., 2012). Nevertheless, a building that has been inundated with PDC deposits, but is largely undamaged, remains uninhabitable for its owner. Damage to trees and other vegetation is typically a function of the temperature and thickness of deposits, i.e. burial, rather than the violent total or partial blowdown or complete removal associated with higher dynamic pressures. As in fast overspill deposits, the concentrated nature of the flow results in a geologically significant poorly sorted deposit up to several metres (e.g., deposits from the 2006 eruption of Merapi were up to 8 m thick; Gertisser et al., 2012), although deposits become thinner (10s of centimetres or more) than the channel-confined parent flow the farther from the parent flow they are found (Charbonnier and Gertisser, 2008). The deposits are generally texturally and compositionally nearly identical to fast overspill deposits, and as a result the speed of an overspill flow is difficult to determine from deposit characteristics alone — in these cases, impacted infrastructure, as well as the extent of a singed zone from the overbank deposits or evidence of a high PDC flow run-up mark on a topographic barrier above the main channel, can be helpful for determining flow velocity (Charbonnier and Gertisser, 2008).

2.3. High-energy surge

High-velocity, low-concentration PDCs are classified as high-energy surges, most commonly represented by directed blast eruptions, column collapse PDCs, and high-energy detached surges that decoupled from their parent PDCs (Fig. 1, top left). Directed blasts typically spread laterally from their source (most often the summit of a volcano) and are frequently generated by the explosion of a summit lava dome, shallow plug, or cryptodome, or through edifice collapse (Bogoyavlenskaya et al., 1985). They can also occur not only as single events but as complex sequences of collapses and directed and funnelled explosions of a rapidly growing lava dome (e.g., Merapi 5 Nov 2010; Komorowski et al., 2013). These directed blasts are unconfined PDCs from their point of origin and tend to cover a very wide range, relatively unaffected by topography or channel confinement (Belousov et al., 2007). Column collapse PDCs form from the gravitational collapse of a sustained ash column, and in many cases are characteristically similar to blast eruptions (e.g., Mt. Lamington, Papua New Guinea 1951; Belousov et al., 2020). By contrast, high-energy detached surges may originally be coupled with a fast-moving dense component and become unconfined by escaping the channel or otherwise changing direction from their parent flows, while maintaining their high velocities and dynamic pressures (e.g., Unzen 1991, Yamamoto et al., 1993). Near source, velocities of directed blasts may be as high as 150 m/s (e.g., Mt. St. Helens 1980; Esposti Ongaro et al., 2011) and typically over 90 m/s (Cole et al., 2015), while high energy detached surges maintain speeds up to those of their parent PDCs (up to ~60 m/s; Yamamoto et al., 1993). The lack of kinematic coupling between high-energy surges and their basal layers allows them to maintain high velocities and travel great distances beyond (or without) their parent flows (Breard, 2016).

Directed blasts frequently have high dynamic pressure (over 10 kPa) close to source and along the primary flow axis, but lower dynamic pressures (less than 1 kPa) in more distal areas (e.g., Jenkins et al., 2013; Gueugneau et al., 2020) and in measured cases have shown temperatures over 300 °C (Cole et al., 2015). This results in a wide range of effects on humans, the built and natural environment, with fatalities and destruction from blunt trauma and thermal impacts in proximal zones, and with injuries and relatively little damage in the peripheral zones. In well documented cases such as the 1631 eruption of Vesuvius, column collapse PDCs displayed many directed blast characteristics, causing near total damage in the most affected areas through high dynamic-pressure and covering a widespread area (Rosi et al., 1993). Similar to blasts, the intensity of these PDCs wanes on the margins, where they can display non-binary impacts, with survival of people and structures indicating characteristics consistent with slow margins of dense PDCs as well as low-energy, dilute surges (Rosi et al., 1993). For example, the 1902 column collapse from La Soufrière, St Vincent, showed extensive damage in areas near source (Anderson and Flett, 1903; Baxter, 1990), but was not capable of overturning trees or sturdy structures by the time it reached heavily inhabited areas, ~8 km from source (Baxter, 1990). Despite this, there were over 1500 deaths as well as nearly 200 hospitalizations (with 80 subsequent deaths) largely from burns and the asphyxiating effects of the ash (Will, 1903; Baxter, 1990). Similarly, in the 8 May 1902 Mount Pelée blast eruption (which had a death toll of ca. 28,000), people in St Pierre, ~8 km from source, were severely burned by PDCs and fires with many laying prone in the "pugilistic attitude" frequently associated with deaths due to temperatures over 200 °C (Anderson and Flett, 1903; Will, 1903; Lacroix, 1904; Baxter, 1990).

Detached pyroclastic surges that decouple from and/or outrun their parent flows can also maintain high dynamic pressure despite their low concentration. These surges are more capable of overcoming topographic barriers than their parent dense PDC, as was the case in the deadly June 1991 Unzen eruption, in which dilute surges detached from their parent flows and outran them by 0.8 km, unexpectedly reaching an inhabited area where 43 people were killed (Nakada and Fujii, 1993). The peak dynamic pressures of these surges were high enough (up to 8 kPa in some parts of the surges; Clarke and Voight, 2000) to destroy 50 houses, flatten trees, and move cars tens of metres (Nakada and Fujii, 1993; Cooper, 2018). Similarly, some high-energy detached surges in the 1994 Merapi eruption maintained dynamic pressures that remained high enough to topple masonry walls, down trees, strip roof tiles, and destroy bamboo huts 5 km from source (Abdurachman et al., 2000), which we estimate requires dynamic pressures of at least 2 kPa. Detached surges during the June 1997 dome collapse eruption of Soufrière Hills volcano were calculated to have velocities over 50 m/s and sufficient dynamic pressure to flatten trees, bend reinforcement bars, and transport large water tanks in areas near the point of detachment (Loughlin et al., 2002b).

Deposits from these dilute, but high energy, surges are generally quite thin, but can reach greater thicknesses in depressions and valleys. Following the Unzen eruption, surge deposits were typically no more than 20 cm thick (Nakada and Fujii, 1993) and were sometimes only a few centimetres thick, in contrast to the up to 10 m thick deposits from the parent flows (Miyahara et al., 1992). Deposits in the 1902 Mt. Pelée blast are estimated to range from 1.5 m along the main flow axis to 30 cm at the margins (Hovey, 1904; Bourdier et al., 1989). Deposits from the 26 December 1997 blast at Soufrière Hills ranged from a few cm to 3 m outside of channels, while deposits were up to several metres thick in river valleys (Sparks et al., 2002; Belousov et al., 2007). High energy blasts often leave a distinctive two-layer deposit (e.g., Soufrière Hills 1997, Sparks et al., 2002; Merapi 2010, Komorowski et al., 2013) consisting of a basal, poorly-sorted, coarse layer that typically includes ripped up clasts of the underlying surface, overlain by a much finer-grained, better sorted deposit with some internal bedding (Brown and Andrews, 2015).

2.4. Low-energy detached surge (LEDS)

LEDS represent the low-velocity, low-concentration end of the unconfined PDC spectrum (Fig. 1, bottom left). These slow-moving surges (~1–2 m/s) represent the upper dilute layer of a PDC that has detached from its dense, basal flow layer (Lube et al., 2011; Cole et al., 2015; Dufek et al., 2015). The dilute nature of these surges combined with their height allows them to easily overcome topographic barriers. In recorded events, these surges are most commonly seen moving laterally from their confined parent flows and escaping channels, leading to unexpected inundation of inhabited areas. How, why, or where along the flow path a surge detaches is typically related to a change in the underlying syn-eruptive topography and/or the pulsative nature of the eruption, which can act to reduce channel capacity or redirect the channel away from the straight-line flow inertia, as described in the Introduction (Sulpizio and Dellino, 2008; Charbonnier and Gertisser, 2011; Ogburn et al., 2014). In contrast to high-energy surges, low-energy surges are typically kinematically coupled to their dense underflow; due to their low density and high temperature, LEDS typically cannot propagate far once they have detached from their parent dense flow (100 s of meters or less), and their thickness should decrease rapidly with distance from the detachment (Breard, 2016).

Due to their low velocity and concentration, and thus low dynamic pressure (typically <2 kPa), LEDS damage to buildings, infrastructure or vegetation is typically minor (with the exception of secondary damage through fire). For example, in the June 1997 Soufrière Hills eruption, while surges close to the point of detachment from the channel-confined flow had high velocities and dynamic pressures, at greater distances the surges were not capable of blowing down trees or poles at distances greater than 2 km from source (Cole et al., 2002). Damage to buildings was caused almost exclusively by temperatures up to around 400 °C (Baxter et al., 2005), indicating greatly decreased dynamic pressures at distance from source (calculated in some places at 0.32 kPa). The impact for humans can range from minor through to fatal burns injuries, with the chances of survival influenced by the LEDS temperature and duration as well as how much skin is exposed by clothing, to what extent the victims breathe in the LEDS, and the availability and timing of medical resources (Baxter, 1990). The bodies of victims in such PDCs often show evidence of brief exposure to extreme heat, with many of the limbs flexed into the "pugilistic attitude" associated with fire and PDC deaths (e.g., Soufrière Hills, June 1997, Merapi 1994: Baxter, 1990; Baxter and Horwell, 2015; Baxter et al., 2017).

Temperatures in these types of surges have been observed to be at least 180 °C and up to over 410 °C based on both direct measurements (Soufrière Hills 1997; Loughlin et al., 2002a, 2002b) and proxy estimates based on damage to vegetation and buildings (Merapi 1994, Voight and Davis, 2000; Unzen 1991, Fujii and Nakada, 1999). In some events a "sear zone" or "singe zone" of charred vegetation was seen to extend up to 25 m beyond the distal margins of surge deposits (Loughlin et al., 2002a).

The deposits of LEDS are characterized by their relative thinness and poor preservation in the long-term geologic record. In most historical cases, these surges have been recorded as thin as a few centimetres and no thicker than 20 cm, even when associated with metres-thick, channel-confined PDCs (e.g., Soufrière Hills 1997; Cole et al., 2002, Druitt et al., 2002; Merapi 1994; Abdurachman et al., 2000; Unzen 1991: Miyahara et al., 1992). Deposits tend to mantle the landscape as a result of settling from the dilute surge (Druitt et al., 2002) and are typically thinnest in open areas (Abdurachman et al., 2000). Most observed deposits are massive and normally graded, generally lacking any internal stratification, but deposits may contain multiple discrete layers if the event involved more than one surge pulse (Abdurachman et al., 2000; Cole et al., 2002; Druitt et al., 2002). In most cases, the deposits are poorly sorted ash but may contain lapilli and rare blocks in addition to gas segregation pipes and mixed in soil and charred wood fragments picked up in transit (Abdurachman et al., 2000; Druitt et al., 2002).

Single eruptive events may contain both high- and low-energy detached surges, as seen in the 1991 Unzen eruption. In the June event, deadly high-energy surges killed 43 people and had dynamic pressures large enough to sweep away cars and trees in one area (Cooper, 2018), while low-energy surges were capable of burning, but not bending or breaking, trees in other areas (Nakada and Fujii, 1993). Similarly, in the September Unzen event, high-energy surges in some locations were powerful enough to sweep away cars and trees damaged in the earlier eruption, while in another location low-energy surges caused damage only though heat, melting vinyl and charring building windows on the volcano-facing side of the buildings (Fujii and Nakada, 1999). Peak dynamic pressures in these events may be up to 8 kPa in the high-energy surges, and lower than 2 kPa in the low-energy surges (Clark and Voight, 2000). In the June 1997 Soufrière Hills eruption, descriptions of surge impacts are indicative of both high- and low-energy surges at different distances from the location of surge detachment, showing a loss in energy with greater distance (Loughlin et al., 2002b).

3. The 2010 Merapi eruption

The full spectrum of confined and unconfined PDCs can occur within one eruption, affecting multiple places at the same time, or the same place at different times. PDCs produced during the 2010 eruption of Merapi in Indonesia provided one such example. Post-eruption field studies of the PDC impacted areas offered a unique opportunity to characterise the range of PDC types, their dynamics, deposits and interaction with populated areas to the south of the volcano. Here, we synthesise the sequence of PDC events and their impacts and present new data for key villages along the Gendol river. We focus on slow overspill flows and low-energy detached surges, as these two unconfined PDC end-members and their impacts are poorly documented in the literature.

After approximately one year of unrest, Merapi volcano began a new eruptive sequence on 26 October 2010 with the explosion of a cryptodome and associated high-energy PDCs laterally directed towards the south. These initial PDCs extended 6.8 km from the summit and killed 35 people who had not evacuated (Jenkins et al., 2013, 2016). Unusually rapid dome growth (to 25 m^3/s), with recurrent explosions and PDCs continued from 29 October until the paroxysm on 5 November (Surono et al., 2012; Pallister et al., 2013; Komorowski et al., 2013; Charbonnier et al., 2013). On 5 November, starting at 00:02 local time (UTC +7), a series of five laterally directed dome explosions occurred, concurrent with retrogressive collapse of the dome, resulting in at least four distinct types of PDC in under 15 min: high-energy unconfined PDCs, dense valley-confined flows, overspill flows, and detached surges (Komorowski et al., 2013). Further gravitational dome collapse, fountain and sub-Plinian column collapse led to PDCs that extended to 15.5 km in the Gendol valley in the south, with flow overspills and low-energy detached surges extending 700 m from the channel and up to 200 m from the parent flow (Charbonnier et al., 2013; Komorowski et al., 2013; Jenkins, et al., 2016). PDC overspill and detachment along the more distal parts of the Gendol channel (>8 km from source) during this paroxysmal phase killed ~170 people (Jenkins et al., 2013, 2016) and damaged ($n = 395$), severely damaged (removed the roof: $n = 108$) or destroyed ($n = 645$) 1148 buildings. This event was termed a 'centennial' eruption (Surono et al., 2012), as this magnitude and style of eruption is seen approximately every 100 years at Merapi.

Field visits to the Merapi area three weeks after the 5 November 2010 event, and several times over the years that followed, allowed some of the authors [SFJ, SJC, JCK, and PJB] to collect detailed field data on confined and unconfined PDCs produced during the eruption. The geology, dynamics and impacts associated with the directed blast that affected a large swathe of the upper flanks to ~8 km from the summit are presented in Komorowski et al. (2013) and Jenkins et al. (2013). Here, we focus on the generation mechanisms, deposits, impacts and inferred dynamics associated with i) slow overspill flows, and ii) low energy detached surges in villages along the Gendol river channel more than 10 km to the south of the summit. Fast overspill flows were also observed along the Gendol, but impacts were total, with all buildings, vegetations and victims buried with no observable remains. Uniquely, our field studies combined geological and engineering expertise in collecting and interpreting data on the deposits and physical impacts of the unconfined PDCs, which could be cross-referenced with medical data on the nature of burns injuries to victims. Some of the geology (Charbonnier et al., 2013; Cronin et al., 2013) and impacts (Jenkins et al., 2013, 2016; Baxter et al., 2017) from these more distal unconfined PDCs during the Merapi 2010 eruption have been discussed previously; here we present data not included in these studies. We hope that these data and interpretations are valuable for emergency management and planning in providing the first multi-disciplinary case study of unconfined PDCs and their impacts.

3.1. Case study sites

We focus on two distinct types of unconfined PDC, for which we discuss the associated generation mechanisms, dynamics, impacts and deposits at two villages (Fig. 2):

- Bakalan, 12.6 km straight-line distance from the summit and on the western edge of the Gendol river channel. The distal slow overspill flow on 5 November inundated 31 buildings within this village, with associated LEDS impacting a further 9; we concentrate on the impacts within the area inundated by the dense flow for this case study. Residents had evacuated the village prior to flow inundation.
- Bronggang village, ~13.5 km from the summit, on the western edge of the Gendol river channel, and bordering a sabo engineering dam bridge that crosses the channel and is part of the lahar management system. During the 5 November paroxysmal phase of the eruption, LEDS impacted 48 buildings in Bronggang, killing 54 people who were in the process of evacuating.

3.2. Slow overspill flow: Bakalan village

3.2.1. Generation

The flow first overspilled the main Gendol channel nearly 2 km upstream to the north, likely because of a bend in the channel towards the east and previous infilling of the channel with PDC deposits emplaced on 4 and 5 November (Charbonnier et al., 2013). Significant narrowing of the channel, and thus a reduction in channel capacity, approximately 1 km to the north upstream of Bakalan village, along with a number of sabo engineering constrictions along the channel, may also have played a role in creating further overspill flows that inundated the village (Fig. 2). Bakalan marks the distal margin of the overspilling flow, with 9 of the 40 buildings in the village affected by LEDS, and 31 by the overspilling flow (Fig. 2).

3.2.2. Impacts

Slow overspill flows up to 2 m thick inundated 6 buildings without destroying, burying or sweeping them away (Fig. 3a-c); a further 8 sustained major damage to the roof and some walls but remained partially standing (Fig. 3d). Less resistant timber outhouses and animal shelters were destroyed by any inundation of dense flow. The gradation of building damage from complete destruction through to buildings remaining standing, despite flow having inundated the building envelope, was gradual but extended over a relatively short distance of ~50 m. Within this zone of rapid damage attenuation, building conditions fell mostly

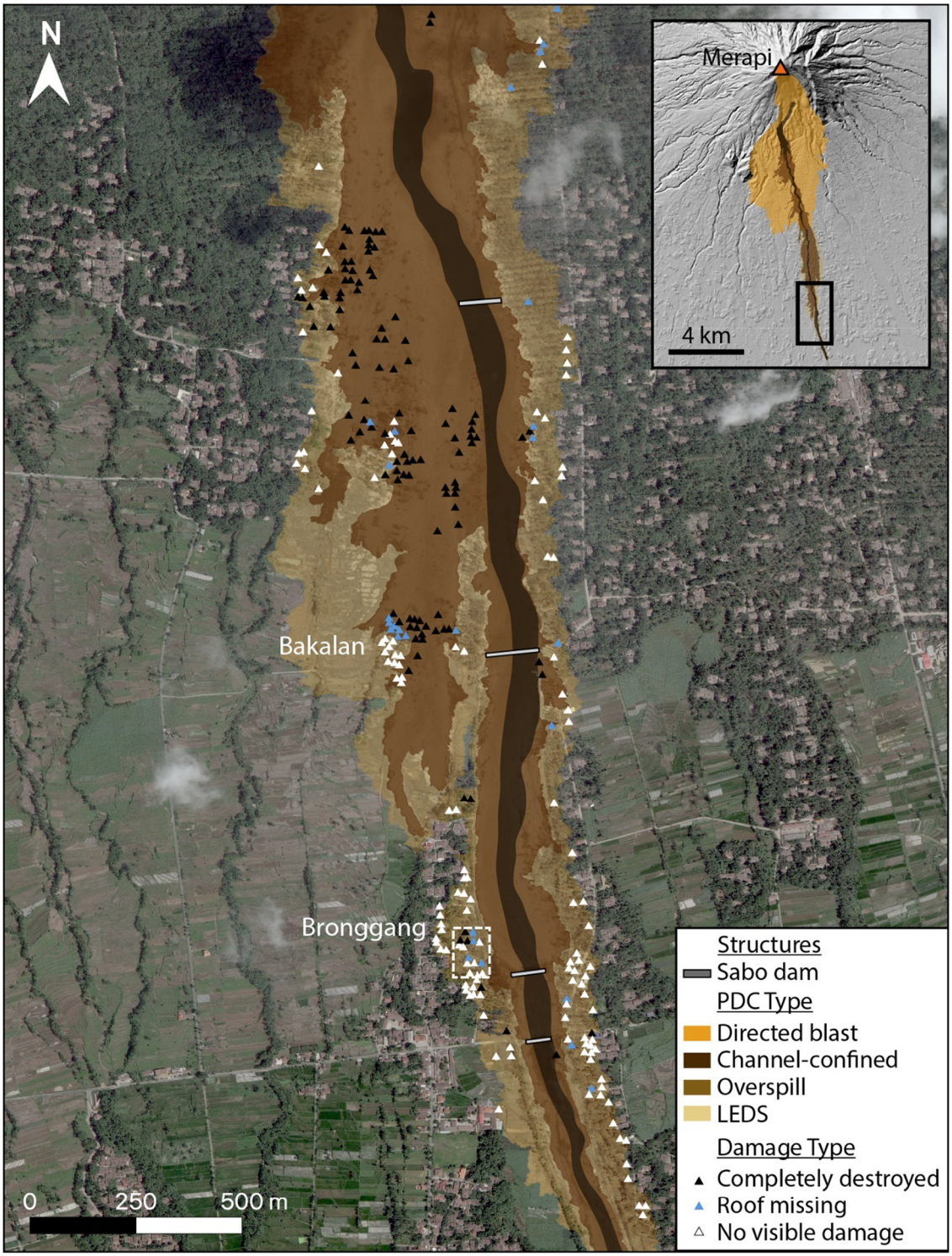

Fig. 2. Channel-confined, overspill and detached PDCs along the Gendol river valley following the 5 November 2010 eruption of Merapi. Coloured triangles indicate level of damage observed in buildings in pre- and post-eruption satellite images (Jenkins et al., 2013). Digital Globe optical Basemap imagery (image acquired 11 Nov, 2010). White box surrounding buildings in Bronggang shows the locations of buildings presented in Fig. 5. Inset shows the village locations relative to the summit and wider PDC impacted area.

into one of two categories (with increasing distance from the parent flow):

1. Inundation with little to no structural damage, although roof tiles, rafters and purlins were lifted from the overhanging portion of the roof facing the flow. Roof tiles were cracked and/or penetrated by larger clasts carried within the dilute component of the PDC (Fig. 3a and b).
2. Dense flow blocked by the walls of buildings, with little to no inundation through openings such as cracked glazing or doors; roof tiles remained unaffected (Fig. 3c).

In addition to these main scenarios, we observed more severe damage where: i) isolated fires had ignited building contents and burned roof supports causing roof failure in one or more rooms, and ii) boulders

Fig. 3. Photos of slow overspill flow impacts in Bakalan village including: a) Thick deposits of up to 2.5 m partially burying houses and causing structural damage on upflow side of structure, b) inundation with minor structural damage, c) flows blocked by building fronts, resulting in little to no inundation, d) severe structural damage caused by large boulders carried by the dense flow. Photos taken 7 December 2010 by S.F. Jenkins.

of up to 1 m diameter carried within the flow caused structural failure of one or more walls (Fig. 3d). Buildings in Bakalan village that were outside of the dense flow overspill and affected only by LEDS sustained similar impacts to those in the Bronggang area (Section 3.3). It is possible that fires observed in the area inundated by the dense flow were ignited by the passing of LEDS that preceded the dense overspill, particularly as fire damage is observed in those buildings in Bakalan that were impacted only by the LEDS. However, any damage caused by the LEDS is expected to be of lesser consequence than that caused by the dense overspill; the brief gap in time between the two PDCs means that the temperature of the LEDS and flows were likely not markedly different, i.e. fires apparently caused by LEDS could also have been caused by the dense overspill flow.

People were evacuated from Bakalan prior to the 5 November event, although locals reported between four and five fatalities in the village.

3.2.3. Deposits

Stratigraphic sections studied after one rainy season in the Bakalan village show a massive, poorly-sorted overspill flow unit with blocks inside an ash-rich matrix, of ~2–3 m thickness overlying three 1–8 cm thick LEDS units at the base. Overbank deposit thicknesses in the Bakalan area vary from 2 to 7 m and two overbank units are present in stratigraphic sections located at the overspill point, ~1 km upstream of the village (Fig. 2). Based on stratigraphic data from the valley-confined PDC deposits collected in the Gendol channel in summer 2011, only two valley-confined PDC units reached that far downstream during the 5 November events (mBLA4 and mBLA5 units in Charbonnier et al., 2013). Based on stratigraphic correlations between the valley-confined and unconfined deposits, only the uppermost valley-confined unit (mBLA5) produced the main overspill flow unit that reached Bakalan, while the lowermost one produced the surge layers found at the base of the unconfined deposit stratigraphy.

3.2.4. Dynamics

The maximum height of the unconfined PDC as it was emplaced remained above 10 m throughout Bakalan, as evidenced by palms and trees that were singed to their full height (e.g., Fig. 3a). Just to the west of the village and on the periphery of the LEDS, partially singed trees suggest maximum current heights for the more dilute component alone of between 5 and 10 m. Much of the structural damage to buildings in the north of Bakalan was the result of isolated high pressures associated with boulders of dome rock carried within the flow (e.g., Fig. 3d). The lack of structural wall failure within the main part of the slow overspill flow suggests dynamic pressures of less than 3 kPa (following the failure calculations of Jenkins et al., 2013). Maximum PDC velocities, assuming a PDC deposit density of 1000–2000 kg/m^3 (Druitt et al., 2002; Lube et al., 2011; Charbonnier and Gertisser, 2012), were relatively slow at 1.7 to 2.5 m/s (Eq. 1):

$$V = \sqrt{\frac{2q}{\rho}} \tag{1}$$

where V = velocity (m/s), q = dynamic pressure (Pa), ρ = density (kg/m^3). Based on impact observations, the overspill flow that entered Bakalan from the north appears to have been relatively low in temperature, at 100 to 200 °C. A number of thermal indicators could be used to infer emplacement temperatures of the LEDS (see Section 3.3.4) while for the dense flows, temperatures were constrained from the

presence of little to no charring or blackening of timber roof supports (<200 °C: Barcík et al., 2014) and the presence of deformed polyethylene plastic pipes within the upper part of the flow deposits (>100 °C). PDC deposits to the south of Bakalan, but closer to the Gendol channel, remained at 180 °C during field studies carried out 34 days after emplacement, supporting the relatively low flow temperatures estimated within Bakalan. These flow temperatures are lower than those observed for the same eruption by Trolese et al. (2018) using charcoal reflectance techniques (240–320 °C). This discrepancy may be explained by temperature heterogeneity within the flow, difference in methods used, and the location of their sampling sites, which were only from within the valley-confined deposits. These temperatures are low relative to some dense unconfined deposits from other eruptions, with deposits from the June 1997 Soufrière Hills eruptions measured in the days to weeks after the event at over 400 °C (Cole et al., 2002), though unconfined deposits from the 2015 dome collapse events at Colima (Mexico) show temperatures from 180 to 220 °C (Pensa et al., 2018). Lower temperatures at Merapi in 2010 may reflect entrainment of air over the long travel distance and interaction of PDCs with dense, tropical vegetation, while other factors could include the relatively small magma volume, the effect of topography in entraining cooler, entrainment of ambient air close to source, and/or the high moisture content of the PDCs due to the summit hydrothermal system saturating the source dome rock (Jenkins et al., 2013; Komorowski et al., 2013; Trolese et al., 2018).

3.3. Low-energy detached surge: Bronggang

3.3.1. Generation

The channel constriction caused by the sabo engineering dam and upstream concrete levees, in addition to a slight bend in the river channel towards the east at the northern edge of Bronggang village (Fig. 2), are thought to have promoted surge detachment from the parent channel-confined flow (Jenkins et al., 2013). LEDS then propagated around 6 to 8 m down the concrete levees and extended laterally 25 to 135 m into Bronggang via three different entry points. Numerous deeply charred logs and embers (firebrands) were left piled up on the top of the concrete sabo walls that run alongside the Gendol channel, marking where the surges detached (Fig. 4). A few small logs were carried down into the villages, potentially bending or knocking down banana trees as they collided into them down the incline. A more concentrated PDC lobe overspilled for a very short distance of about 20 m directly over the highest part of the sabo wall but at the location of maximum channel curvature, where the levees constrict at a 45° angle towards the centre of the Gendol river channel. Although the presence of this wall and constriction in the channel strongly controlled and even triggered early PDC overspill into the lower part of Bronggang, our fieldwork showed that only three out of four or potentially five surges associated with valley-confined PDCs overspilled at that location.

3.3.2. Impacts

Direct damage from the LEDS was minimal, with buildings remaining largely intact but interior and exterior plastic melted, furniture charred and paper singed. Although the LEDS were not hot enough to directly ignite these flammable objects, fire was the cause of total and partial destruction of buildings in the village. Of the 48 buildings impacted by LEDS in Bronggang, seven timber buildings were completely destroyed and a further five masonry buildings, with timber frame and tiled roofs, partially destroyed, all by fire rather than direct damage from the LEDS (Fig. 5a). Firebrands (embers from burning logs within the parent PDC) carried within the surge ignited flammable materials such as hay in animal sheds and sticks and coconut husks in outside lean-to wooden kitchens (Fig. 5b), with fires beginning in these flimsy wooden structures and then rapidly spreading into the adjacent houses. The large ventilation gaps also allowed firebrands to travel with the ash inside several houses, as evidenced by ignited mattresses or sofas, which smouldered without causing the houses to catch fire (Fig. 5c). In one building, a small rupture in the gas tank of a motorbike stored inside greatly increased the availability of fuel leading to a fire that completely destroyed the building.

Prior to the eruption, ~400,000 people were rapidly evacuated to emergency shelters (Surono et al., 2012), and ~1 million were otherwise displaced (Lavigne et al., 2011), but in distal villages like Bronggang many people had not evacuated at the time of the paroxysm. Out of 59 people remaining in the surge zone, all of whom received burns, there were only 5 survivors. Those who were caught outside had little protection and most would have died instantly (Baxter et al., 2017); however, large ventilation pathways meant that the LEDS readily entered buildings and twenty-five bodies were retrieved by rescuers from inside houses. A further 18 bodies were found outside, and 11 others died in, or on the way to, hospital (Fig. 5a, Jenkins et al., 2013; Baxter et al., 2017). Some of the victims received burns from running in the deposits as they tried to escape and a cow was found alive at the time of the first rescue mission, approximately two hours after

Fig. 4. Photos taken from the top of the concrete levee bordering the Gendol and adjacent to Bronggang village: a) Looking southwest down the levee and in the direction of LEDS spillover into Bronggang village; b) Looking north up the infilled Gendol channel with LEDS and small flow overspill into Bronggang to the left of the image. Charred tree branches and embers (firebrands) that were carried within the PDC can be seen on top of and within deposits in the channel and in the village. Photos taken by S.F. Jenkins 25 days after impact on 30 November 2010.

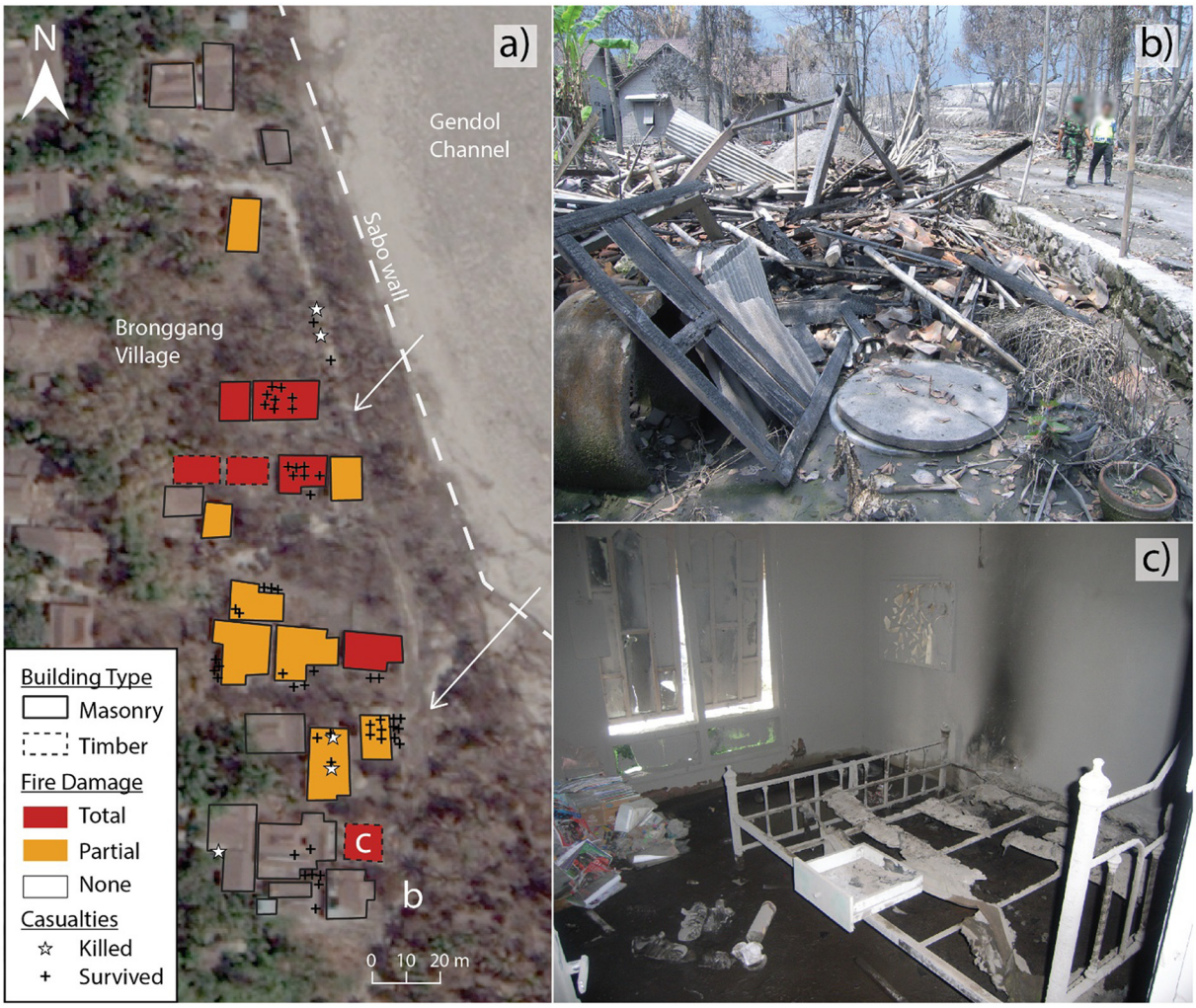

Fig. 5. a) Spatial distribution of building type, fire damage and casualties in a section of Bronggang village (inset in Fig. 2), ~13.5 km from the summit and subject to LEDS. LEDS flow direction across sabo walls is indicated by white arrows with the white dashed line marking the sabo concrete levees bordering the Gendol channel, b) remains of a burned and charred timber-framed building that was totally destroyed by fires caused by LEDS (Photo taken by S.F. Jenkins 28 days after impact on 3 December 2010), c) straw mattress burned by an isolated fire as a result of LEDS inundation (Photo taken by S.F. Jenkins 29 days after impact on 4 December 2010). The location of the images in (b) and (c) are marked by the corresponding letters in (a).

impact, but subsequently died. The last living person was rescued by approximately 06:00 (local time). Specifics of the injuries suffered by the burn victims are described in medical detail by Baxter et al. (2017). Survival of hospitalized patients was tied closely to quality of medical care, as resources in some cases were insufficient (e.g., ventilators for treating inhalation injuries) (Baxter et al., 2017).

3.3.3. Deposits

We identified a complex stratigraphy at the base of the sabo wall, just inside the village of Bronggang, consisting of four different main depositional units (Fig. 6):

- At the base of the sequence, there were patches of dry very fine grained, very well-sorted, loose grey ashfall deposit 1 cm thick, which we interpreted as pre-5 November tephra erupted between 26 October and 4 November. This overlays pre-eruption soil and vegetation.
- The next unit was whitish-grey massive, coarse to fine ash, loose, poorly sorted and 3–4 cm thick with chunks of charcoal and a burnt odour. We interpreted this unit as a LEDS deposit contemporaneous or correlated to one of the surge units seen in the main Gendol channel. This unit contained pieces of aluminium foil, house tiles, and dried to scorched leaves. It was overlain by a 2 cm thick very fine-grained pinkish-tan ashfall layer.
- The third unit was a dark grey, fine ash, massive, well-sorted and normally graded 4 cm thick unit with chunks of charcoal and a locally erosive lower contact. We interpreted this unit as a second LEDS deposit contemporaneous or correlated to one of the surge units seen in the main Gendol channel. It was again overlain by a 1 cm thick, very fine grained, pinkish-tan, ashfall layer.
- The uppermost unit was a very poorly sorted, massive, compact, pinkish brown, normally to symmetrically and even reversely graded, 35–45 cm thick fines-rich unit. This unit contained large dense clasts up to 23 cm in diameter scattered on the top surface and also formed a central coarser clast-rich zone with a more pinkish matrix. We interpreted this unit as resulting from a minor overspill lobe of a valley-confined, block-rich PDC. Field evidence suggests that this PDC was not very mobile and was stopped by the ~30 cm tall stone-wall curb of the main village road on the Gendol side (Fig. 6). This unit was correlative and thickened to a 93 cm thick sequence directly on top of the sabo wall. It was overlain by a 5–6 cm thick, very well-sorted, massive, fine pinkish tan ashfall layer with a vesicular texture and perhaps some poorly preserved accretionary lapilli.

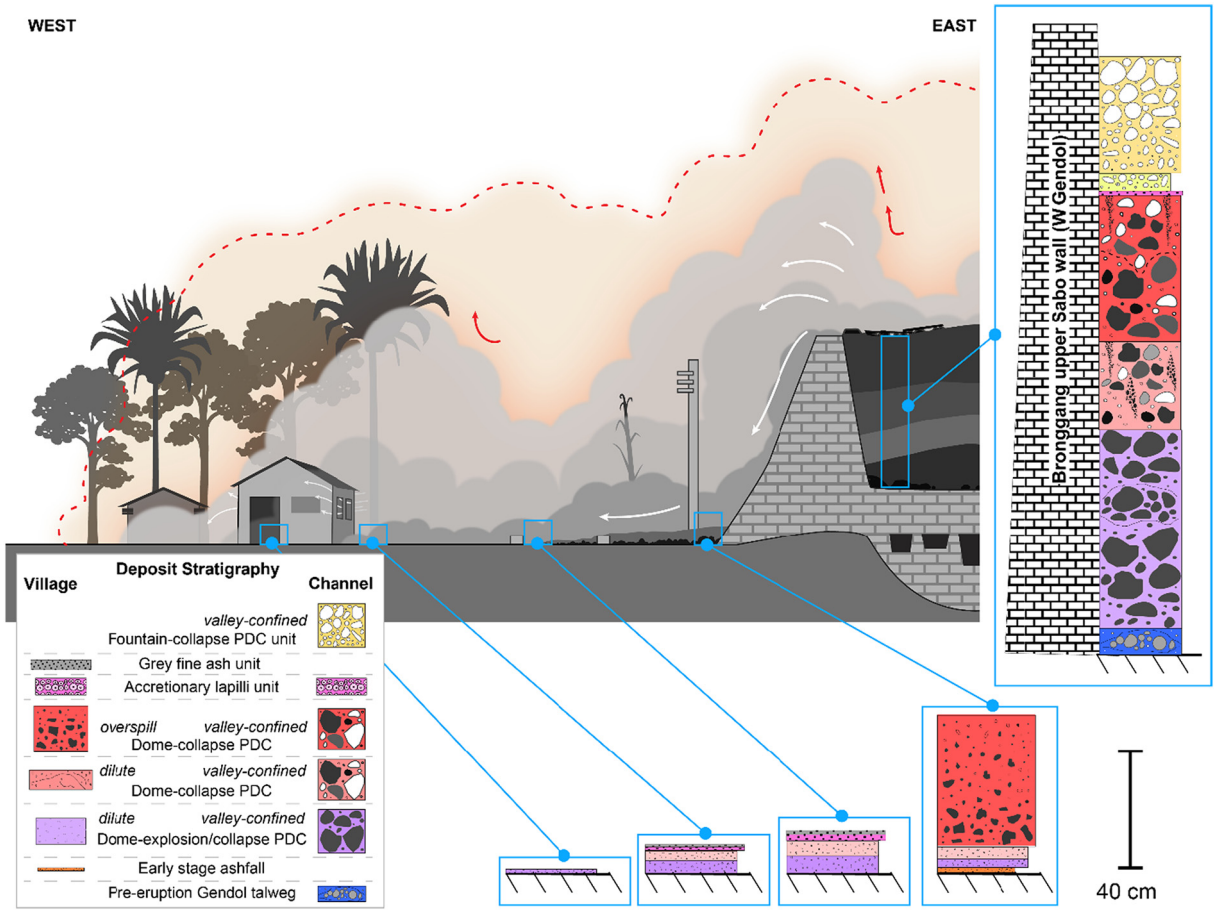

Fig. 6. Schematic demonstrating the dynamics of LEDS as it leaves the channel and inundates Bronggang with stratigraphy of channel-confined, overspill and LEDS deposits in and adjacent to Bronggang, ~13.5 km from the volcano summit.

We interpreted these deposits as representing three different minor PDC overspills, and associated ash cloud fallout, from the Gendol main channel: the lower two represent deposition from the dilute surge component only, while the upper unit includes deposition from the dense flow component as well, although this did not propagate as far as where the buildings are in the village. Parent PDCs remained largely channelized in the Gendol. LEDS depositional units were visible outside of the buildings, although only the very fine ash component of LEDS infiltrated inside (Fig. 6). The very fine ash that had infiltrated the houses was highly fluidized and inflated even 3 weeks after emplacement. A very substantial proportion of the infiltrated ash was fine enough to be inhalable by any occupants (22.1 wt% less than 15 microns) and capable of reaching the main and smallest airways of the lungs (<16.8 wt% and <9.0 wt% respectively). This material on arrival would have been suspended in the atmosphere in the room in sufficient concentration to be impossible to avoid breathing into the lungs. The coarser fraction would be rapidly deposited and was hot enough to cause severe skin burns. No stratification in deposits could be seen inside the buildings, suggesting that only one of the LEDS infiltrated, or the material was lofted and well dispersed so that it settled out gradually into one massive unit of up to 2 cm thickness that coated items inside the building (Fig. 6).

3.3.4. Dynamics

Evidence from the height of scorching on trees in the village indicated that the dilute current was at most about 8–10 m high above the village (2 to 4 m above the levee tops). While trailing wakes from the PDC surge which are no longer part of the moving current can sometimes singe trees at greater heights than the original current, adding uncertainty to these numbers, this added height is still relevant for both hazard and overspill dynamics. In Bronggang, at the base of the concrete levee bordering the Gendol channel, a concrete utility pole of ~7.5 m high showed pockmarks, from small clasts within the LEDS striking the pole, of ~10–20 mm diameter and a few mm deep along the full height of the pole on the upflow side (Fig. 7a). The boundary between the area of scorched, dried vegetation and pristine vegetation was very sharp, developing over less than 1 m. Fig. 7b shows a traditional Javanese building at the very periphery of the LEDS affected area in Bronggang, where ash adhered to the wall of the building facing the flow, and nearby vegetation dried and singed to a height of approximately 5 m, with some tiles dislodged on the roof overhang. Vegetation and building components to the side and back of the building (farther from the flow) were unaffected. Thus, at the edge of the surge, as evidenced by the vegetation patterns (Fig. 7b), the maximum LEDS height was still about 5 m. Taking the maximum LEDS height of 8–10 m and maximum deposit thicknesses of ~4 cm (Section 3.3.3) gives a crude estimated maximum LEDS density of ~4 to 8 kg/m^3 (assuming a 1000–2000 kg/m^3 deposit density; Druitt et al., 2002; Lube et al., 2011; Charbonnier and Gertisser, 2012). Previous estimates of LEDS densities are rare, but for comparison, Druitt et al. (2002) estimated that in the June 1997 Soufrière Hills eruption, LEDS moving at up to 20 m/s likely had a density of 1.4 kg/m^3 and a particle concentration below 0.1 vol%, and Bursik et al. (1998) estimated distal surges in the 1980 Mt. St. Helens eruption to have a density of 1.5 kg/m^3.

Fig. 7. a) ~7.5 m high concrete utility pole at the base of the concrete levee bordering the Gendol channel showing pockmarks on the upflow side, from small clasts carried within the LEDS striking the pole; b) Traditional Javanese building at the edge of Bronggang village showing the very sharp LEDS boundary, with ash and dried vegetation from the LEDS visible on just the upflow (left of image) wall and surrounds; c) Roof tiles lifted on the overhang of a building facing the direction of LEDS overspill suggesting dynamic pressures of ~0.1 to 0.2 kPa; d) Corrugated plastic roofing sheets melted by the LEDS and/or the deposits suggesting temperatures of at least 100 °C sustained for ~three minutes. Photos taken by S.F. Jenkins, November 2010.

Maximum velocities of 10 m/s for the LEDS as they spilled over the concrete levee can be derived by applying the super-elevation equation (Eq. 2) to the estimated 5 m high concrete levee that would need to have been overbanked by the LEDS associated with the first overspilling PDC in the Gendol. This represents the maximum possible velocity of the LEDS at their point of overspill from the channel—in reality, the LEDS would likely have had lower velocities as they entered the village. Subsequent LEDS would have required lower velocities in order to overspill after previous PDCs infilled the channel, and the LEDS velocity likely rapidly attenuated with distance away from the channel. At the site of overspill, a peak velocity of 10 m/s correlates to a maximum dynamic pressure of ~0.2 to 0.4 kPa, assuming the previously estimated density of ~4 to 8 kg/m^3. These values represent upper estimates as the pre-PDC channel infill likely banked up on the western wall of the channel, so that the overspill height is overestimated. These pressures are consistent with lack of significant tree blowdown, as even minor blowdown requires 0.5–0.8 kPa of dynamic pressure (Valentine, 1998), which at our estimated densities would require a minimum velocity of ~11–16 m/s to generate.

$$V = \sqrt{2gh} \tag{2}$$

where V = velocity (m/s), g = gravity (m/s^2), h = height of barrier to overcome (m).

Some of the standing trees within the village showed light blackening of the bark on the side facing the surge, and their leaves were killed, but the branches remained intact reflecting the low dynamic pressures. Buildings showed limited evidence of mechanical impact: tiles on overhanging parts of roofs facing the channel were blown off by the LEDS being deflected upwards as it hit the wall (Fig. 7c). For only the tiles on the overhang to be lifted, the pressure upwards must exceed the weight of the tile in this location but not in other parts of the roof (BSI, 1996), which we calculate required dynamic pressure of 0.1 to 0.2 kPa. Similarly, low dynamic pressure values can be calculated for the concrete utility pole to remain upright (<0.5 kPa) and a small number of palm trees to be beheaded but not felled (< 0.5 kPa: Jenkins et al., 2013). There was likely a rapid drop off in pressures as the LEDS moved laterally farther from the channel, with no evidence of elevated pressures beyond 40 m. LEDS in Bronggang were therefore not very turbulent given the low dynamic pressures and limited lateral propagation.

Evidence for the thermal effects of the LEDS was complicated by the presence of fires (Fig. 5), but a number of effects to objects away from the fires could be used to narrow down a likely LEDS temperature of 200 to 300 °C: i) Window glass cracked but did not melt (70 to 700 °C); ii) Healthy vegetation dried and singed, but did not ignite (100 to 400 °C); iii) Casualties suffered deep burns to uncovered skin (>150 °C: Baxter et al., 2017); iv) Acrylic roof sheets deformed (>160 °C) (Fig. 7d); v) Thinner nylon clothes melted but did not autoignite (200 to 300 °C). This temperature range is low compared to some instances of LEDS recorded at other volcanoes (e.g., LEDS in the June 1997 Soufrière Hills eruption likely reached temperatures over 400 °C; Loughlin et al., 2002a), though similar to LEDS temperatures estimated in the 1994 Merapi eruption (Voight and Davis, 2000). Possible reasons for the lower temperature LEDS in this eruption likely mirror the reasons for lower temperature overspill deposits, as discussed in Section 3.2.4.

The multi-disciplinary analysis of the Merapi 2010 eruption (Jenkins et al., 2013; Komorowski et al., 2013) was the first of its kind making use of geological, engineering and medical expertise together to reconstruct PDC dynamics. The eruption also differed from prior eruptions because of the sheer number of social and professional media images of the impacts that became immediately available. These remotely sourced images, plus satellite imagery, provided a valuable source of additional information that could be evaluated to: i) infer conditions and impacts as close to the time of PDC inundation as possible, ii) assess impacts over the total PDC impacted area of ~22 km^2, and iii) identify locations where field studies should focus. We were able to apply the lessons learned from the remote and field assessment of Merapi's unconfined PDCs to make a similar assessment of unconfined PDCs produced by the Fuego 2018 eruption in Guatemala.

4. The 2018 Volcán de Fuego eruption

Unconfined PDCs during the Fuego 2018 eruption in Guatemala destroyed an estimated 750 buildings in areas within 8.5 km of the volcano and resulted in at least 332 people killed or missing (with independent estimates of up to 2900 deaths) (Naismith et al., 2020). The Fuego eruption of 3 June 2018 began at 06:00 local time (UTC-6) with paroxysms from the summit vent and PDCs traveling down the western flanks, largely consistent with the volcano's previous eruptive history (Naismith et al., 2019; Pardini et al., 2019). Activity intensified by 12:00 local time, generating a series of PDCs that propagated over 11 km down Barranca Las Lajas to the southeast between 14:00 and 16:00 (Naismith et al., 2019). The flow volume could not be contained by the barranca and overspilled the eastern banks of the Las Lajas channel at ~7 km from the summit at the site of La Reunión golf resort, which had been previously evacuated, as well as the western bank of the channel at ~8 km from the summit, where the channel constricted and there was a sharp bend towards the east. This latter overspill inundated the village of San Miguel Los Lotes (located at ~9 km from the summit), which was still inhabited at the time (Ferrés and Escobar Wolf, 2018; Flynn and Ramsey, 2020). As the PDC struck on a Sunday, many people were congregated at church or at homes and were not working outside of the town. Further PDCs in the Barranca Las Lajas hampered rescue operations two days later on 5 June but remained contained within the channel. Fifty badly burnt casualties caught in dilute PDCs were admitted to hospital, with some urgently transferred by air for treatment in specialist hospitals in the USA and Mexico.

A field assessment of deposits from the 2018 Fuego eruption in San Migues los Lotes, La Reunión, and the adjacent channels was carried out in August 2018, ~3 months after the May eruption [by SJC]. The focus of the field visit was on geological deposits, but ancillary information on impacts was collected where possible, mostly in the form of photographs and field notes. A health-focused assessment was undertaken in June 2018 at the invitation the Pan-American Health Organization [by PJB]. As with Merapi, there were a large number of - sometimes graphic - images available from social and professional media in the hours, days and weeks following the June 2018 PDCs. We collected as many images as possible, broadly categorising them into deposits, impacts and casualties, and further cataloguing each image according to information it may provide regarding PDC dynamics such as velocity, dynamic pressure or temperature. We also used pre- (March 2018) and post-eruption (November 2018) Google Earth satellite imagery, and georeferenced high-resolution satellite images acquired in the days following the eruption and made available online (e.g., Digital Globe imagery acquired on June 7, 2018: White, 2018) to map pre-eruption building locations, and subsequent post-eruption damage. We followed the damage categories applied by Jenkins et al. (2013) for Merapi: Totally Destroyed (TD) where the building was not visible in post-eruption images, Partially Damaged (PD) where some of the building structure remained and could be seen in post-eruption images, and No Visible Structural Damage (NVSD) for buildings that appeared unaffected in satellite imagery. A total of 125 TD, 35 PD and 95 NVSD buildings were observed across La Reunión golf resort (3 TD, 8 PD, 47 NVSD) and San Miguel Los Lotes (122 TD, 27 PD, 48 NVSD) (Fig. 8). The later Google Earth imagery, acquired ~5 months after the eruption, showed that most roofing material (metal sheets) in San Miguel Los Lotes had been scavenged from PD and NVSD buildings in the intervening months (Fig. 8a). From satellite and media imagery of the two overspill locations, we were able to identify at least two types of unconfined PDC, and their impact:

1. Overspill flows, of variable speed, which contained large (>2 m diameter) boulders that caused non-uniform building damage, and were responsible for almost all buildings in the TD and PD categories at both locations, with media images indicating a small number of buildings may have been inundated without causing damage;
2. Low-Energy Detached Surges (LEDS), which for the most part caused little thermal or mechanical damage, resulting in primarily buildings in the NVSD category, even though they were still fatal for at least some of the victims caught in them.

4.1. Impacts

At La Reunión golf resort, the main club building was partially inundated with unconfined PDC deposits and appears to have obstructed the dense component of the PDC, with only isolated lobes of the dense flow extending downflow towards the southeast onto the golf course (Fig. 9c). The main clubhouse sustained structural damage on the upflow side (Fig. 9c), and some individual residences sustained partial damage from fires that caused roof collapse, but only three buildings were totally destroyed, two of which were less than 50 m from the channel edge (Fig. 8b). Inside buildings, there was evidence of slow overspill flow inundation that left deposits of 80 cm or more, with associated surges that left deposits of a few centimetres (Fig. 9b). Media images (22 June 2018) showed subsequent inundation of lahars and debris that left ~50 cm-thick deposits and moved chairs and tables: these could be distinguished from PDC deposits in media images by: i) the increased debris (e.g., branches, bricks) that they carried, ii) evidence of deposit surface remobilisation, iii) that they were clearly wet in comparison with photos of pristine PDC deposits, and iv) the correlation with mechanical impact above the flow (lahars not imparting any mechanical impact above their flow surface: Fig. 9a).

Approximately two-thirds of the northwestern area of the village of San Miguel Los Lotes was almost totally destroyed by overbank PDCs on 3 June (Fig. 8a), which contained large boulders many metres in diameter inside an ash matrix and left massive, poorly sorted deposits up to 2 or more metres deep (Fig. 9d and 9e). A small number of buildings at the northern end of the town escaped total destruction, and buildings at the edge of the zone of total destruction towards the south and east of the town mostly suffered partial damage, but their structures were still identifiable on satellite imagery (Fig. 8a). The portion of the main road running along the south-east and east side of the town (RN-14) was completely inundated, although access to the very southernmost part of the village was maintained.

Most buildings at the golf course and at the far southern and eastern periphery of San Miguel Los Lotes remained relatively intact with no damage visible in satellite imagery. Media images taken during rescue operations show that people died in LEDS affected areas in San Miguel Los Lotes where there was little thermal or mechanical damage to buildings. However, the majority of casualties in the village were buried inside the thick overbank PDC deposits that entered houses and buildings, creating issues to recover the bodies and correctly evaluate the human impact of the eruption.

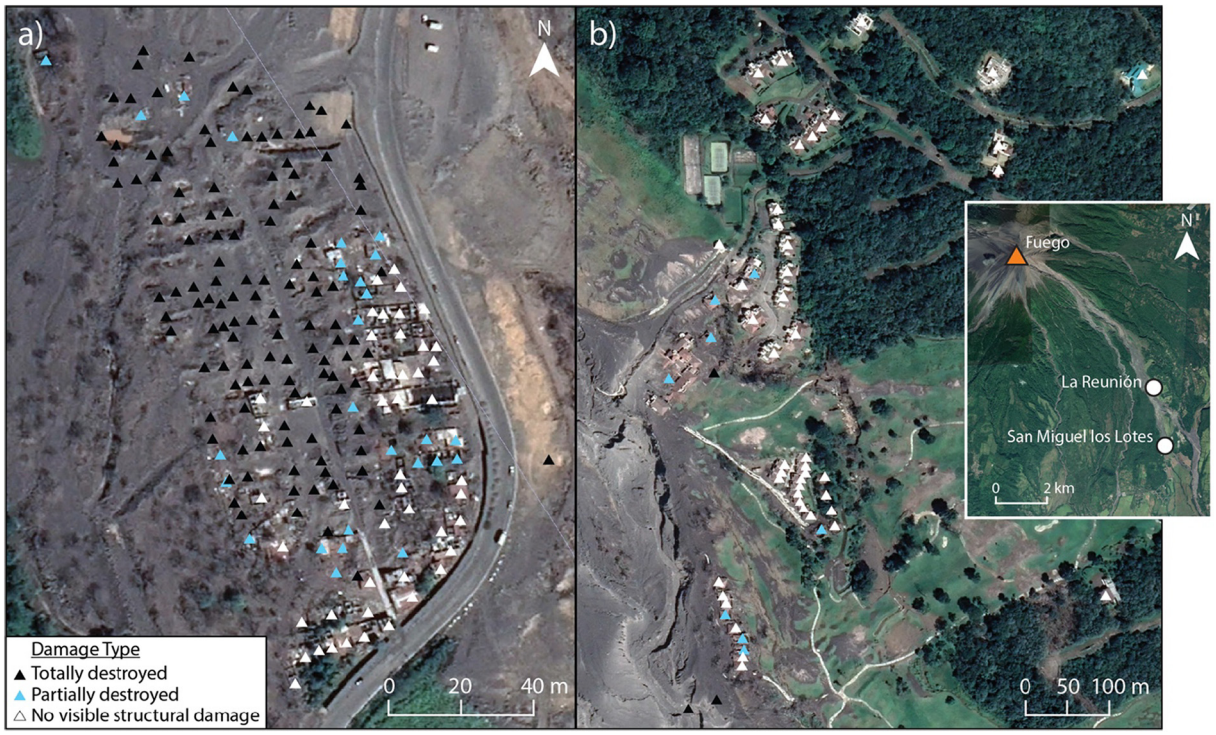

Fig. 8. Remotely mapped building damage for the two main flow overspill locations of a) San Miguel Los Lotes, and b) La Reunión golf resort, following the Fuego 2018 eruption. Google Earth satellite imagery from November 2018 is shown although we assessed damage using a range of remote sourced imagery. Inset shows locations relative to Fuego volcano.

4.2. Inferred dynamics

The maximum height of the PDCs was not easy to determine from media images. There were a number of tall (>10 m) trees in both affected areas that appear singed by the PDC, implying a maximum current height of more than 10 m as the PDC entered the town and golf resort. Media videos of the PDC flowing past a bridge in the adjacent channel just to the south of San Miguel Los Lotes suggest that current heights maintained similar heights in the channel. However, trees in the southern half of San Miguel Los Lotes and towards the peripheries of impacted areas at La Reunión golf resort were not singed to their full height, with canopies still showing as green and unaffected in satellite imagery while the full height of buildings was affected. Thus, the maximum PDC height decreased from >10 m to between 2 and 10 m as the flow slowed down and came to a stop.

At the golf resort, the energy of the overspill flows was low enough that they could be largely blocked by buildings, and where the flows entered buildings, they only moved objects such as chairs a few tens of centimetres away with the associated surges leaving countertop items such as bottles coated in ash but upright (Fig. 9a). This suggests that both the dense and dilute PDC components were traveling at ~1 m/s (certainly less then 5 m/s based on the categories outlined in Fig. 1) with minimal dynamic pressures (<0.2 kPa). LEDS at the golf resort maintained similarly low velocities and dynamic pressures, evidenced by their ability to fell only slim and very small (2–3 m height) trees or palms, but not to remove roof tiles or to move items located on tables inside buildings. Some media images showed wall and roof damage at the golf resort, and field investigation confirmed structural damage to the main clubhouse from PDCs, while most of this damage to other buildings seemed to be the result of post-eruption lahars (wall damage) and fire events (roof damage), rather than direct damage from PDCs (Fig. 9b).

In San Miguel Los Lotes, the overspill flows likely decreased in velocity and dynamic pressure as they moved south and east in order for the buildings in these parts of town to sustain minimal to no observable damage (Fig. 9e). The widespread destruction of most buildings at the northern part of the town along with a few surviving buildings of the same typology (Fig. 8a) suggests that destruction of buildings was caused by a combination of dynamic pressure and missile damage from large clasts carried by the flows. Many large boulders of 2 m diameter or more can be seen in and near the north end of town in post-eruption photos (Fig. 9d) and satellite imagery. LEDS in San Miguel Los Lotes appeared to have low velocity and dynamic pressure (<0.5 kPa), evidenced by the fact that many trees (including palms) within the village remained standing and metal roof sheets remained attached to the roof framing after the event (Fig. 9e).

Isolated fire damage could be seen in some of the buildings at the golf course and in San Miguel Los Lotes, leading to partial or total roof collapse in places. It is not clear from remotely derived imagery if isolated fires were the result of embers (firebrands) carried within the PDC, as at Merapi, or related to the heat of the deposits. Flow deposits at Fuego contained large boulders, but field studies showed that most of these boulders were not juvenile, and therefore unlikely to have provided a concentrated heat source that may also have triggered fire.

Photos from the rescue operation in San Migues los Lotes show that the PDC deposits were hot enough that it was necessary for responders to lay boards down to walk on in some locations, and there were reports of responder's shoe soles melting (World Bank, 2018). These suggest deposits of at least 100 °C, but likely much higher. In one media photo from the interior of a golf course building, chair bases and plastic ceiling fans were melted, and we infer this is the result of radiant heat from the flow deposit rather than the heat associated with the surge (Fig. 9b). For LEDS, media photos from both the golf course and the town indicate relatively low temperatures for the most part (maximum 100–200 °C). Fragile items such as plastic plant pots and bags are not deformed or melted, and in available media images there is no evidence for cracked glasses and only very slight melting to thin nylon clothing (>70 °C). Additionally, media images showed plants that remained alive, and were not dried out, singed or charred by the passing LEDS. This suggests temperatures of around 100 °C or less, significantly lower than in more

Fig. 9. a) inside of La Reunión clubhouse building showing effect of LEDS (ash-covered bottles on counter) and post-eruption lahars (knocked over chairs) (22 June 2018), b) inside of clubhouse building showing overspill deposits to chair height, LEDS deposits of a few centimetres on tables, isolated fire damage to roof, and ceiling fan melted due to radiant heat from overspill deposits (22 June 2018); c) Digital Globe satellite imagery of La Reunión golf resort (acquired three days after impact on 6 June 2018) showing partially inundated clubhouse building. Different shade of grey between left and right side of the buildings shows deposition areas of dense overspill flows (L) which were stopped by structures and LEDS (R) which were able to flow past (adapted from imagery provided by Maxar Technologies under CC BY-NC 4.0); d) aerial photo of San Miguel Los Lotes, facing south, showing fully destroyed northern end of town (bottom of frame) with large boulders, contrasted with mostly undamaged buildings at the south end of town (top left of frame) (AP, 5 June 2018), e) buried buildings in the town of San Miguel Los Lotes showing minimal structural damage and deposits surrounding and on top of buildings (P. J. Baxter, 25 June 2018).

proximal areas (<5 km), where photos from the field studies show significant singing and burning of trees and coffee plants. However, by contrast, some media images showed casualties in a pugilistic attitude with clothing intact, indicating fourth degree burns that have penetrated below the skin layer to involve the limb muscles (at least 200 °C) (Baxter, 1990). Not all casualties shown in media images displayed this attitude, despite wearing similar clothing (t-shirt and trousers) and being affected by LEDS in the same town. Since there was no observed evidence of fires near these casualties, the temperatures necessary to cause these injuries can be attributed to the LEDS. The evidence from thermal effects therefore suggests that there was variability in temperature and/or duration of the impact across the impacted area, reflecting the uneven inundation of PDCs across the village area.

While remotely assessing impacts visible in satellite, aerial and media images in this case study was valuable, access to photos and on-the-ground experience in the aftermath of the Fuego eruption provided vital detail that allowed us to confirm or refute inferences made from media images and added information not visible in remote imagery. Ideally, remote and field approaches are combined, with remote approaches providing information on the immediate post-impact situation and for areas that cannot be easily accessed as well as

providing the larger scale overview, which can then be refined and ground-truthed with informed field visits that provide more detailed information, background and context. Studies relating impacts and PDC dynamics with the deposits provide an evidence base from which likely PDC dynamics and impacts can be forecast. This is particularly important for volcanoes where there are no data on past eruptions, or where the only data available are past deposits.

5. Discussion and conclusions

In this study, we reviewed the physical characteristics and devastating impact associated with unconfined PDCs. We identified four unconfined PDC end-member types: i) Fast overspill flow; ii) Slow overspill flow; iii) High energy surge; and iv) Low energy detached surge, all four of which were produced by the 2010 Merapi eruption, Indonesia. We used previously unpublished data on the deposits and impacts of slow overspill flows in Bakalan village, 12.6 km from the summit, and LEDS in Bronggang village, 13.5 km from the summit, to infer some key characteristics of their emplacement dynamics. Using the lessons learned from Merapi, we then applied the same approach using remotely sourced imagery (satellite images, social and professional media) and field studies to assess impacts and infer the dynamics of unconfined PDCs produced during the Fuego 2018 eruption. The deposits, impacts and dynamics associated with the unconfined slow overspill flows and low energy detached surges produced during the case study eruptions of Merapi and Fuego fall within the range of those observed or inferred in previously recorded events (Table 1 and Section 2). Broad conclusions can thus be drawn about the key characteristics and impacts of unconfined PDCs:

1. Destruction of buildings, vegetation and infrastructure is typically complete in the main path of fast overspill flows and high-energy surges;
2. A rapid attenuation in velocity at the peripheries of flow overspills and high-energy surges leads to reduced dynamic pressures and thus reduced mechanical impact and severity of damage. At the very peripheries of flows (slow overspill flow margin), deposits bank up against the sides of buildings or inundate the interior through open doors without causing any structural damage;
3. Low-energy detached surges are unique amongst the four unconfined PDC types in that they cause relatively little damage through dynamic pressures and leave little geological evidence; however, they are still mostly fatal because of the heat flux and should therefore be afforded the same consideration for hazard management and planning as the unconfined dense flows and high-energy surges for which we may have more geological evidence;
4. The temperature of unconfined PDCs can vary greatly between eruptions, as a function of one or more of the PDC volume, generation mechanism and transport path, as well as the presence of heat sinks such as wet vegetation;
5. General patterns of reduced or little damage in areas where dynamic pressures were relatively low were disrupted by isolated instances of total building damage as a result of fires or boulders/debris transported by the flow.

Unconfined PDCs exist on a spectrum of both concentration and velocity, which both contribute to dynamic pressure, a key trait in determining the damage caused by a PDC. However, the temperature and duration of impact is also an important component in determining impact for the less energetic PDCs. These two factors affect the chance of survival and the probability of fire ignition. It is nearly impossible to disentangle the contribution of temperature and duration in determining thermal impact. Evidence from casualties in Bronggang affected by the LEDS of Merapi 2010, suggests a LEDS duration in the region of minutes (Baxter et al., 2017; Jenkins et al., 2013). Refining estimates of duration

Table 1
The range of unconfined PDC characteristics and dynamics for each unconfined PDC type from previous eruptions following the studies reported in Section 1 and 2 and this study. Values obtained for the four detailed study areas of the Merapi 2010 and Fuego 2018 eruptions are shown in brackets. Distances are straight-line and represent the shortest distance from impact site to summit or channel, and not necessarily the distance travelled.

Deposit thickness (at impact sites)	Dynamics				Distance to impact site	
	Maximum height	Peak velocity	Peak dynamic pressure	Temperature	From summit	From channel
Fast overspill flow						
10s of centimetres[a] to metres[c]	–	30 m/s to 60 m/s	Up to 100 kPa proximal, 15 kPa distal[d]	Up to >600 °C[a]	5 km[a,c]	600 m[c] to 800 m[a]
Slow overspill flow margin						
Up to 0.5 m[e] [Up to ~2 m[a], up to ~3 m[b]]	2 m[b] to 10 m[a,b] [10 m[a], 2–10 m[b]]	1 m/s[e] to 2.5 m/s[a] [~2.5 m/s[a], ~1 m/s[b]]	<0.5 kPa[b] to 3 kPa[a,e] [<3 kPa[a], <0.5 kPa[b]]	100 °C[a] to 410 °C[e] [100–200 °C[a], >100 °C[b]]	2 km[e] to 12.6 km[a] [12.6 km[a], 7 km[b]]	200 m[b] to 300 m[a] [300 m[a], 200 m[b]]
High-energy surge						
<20 cm[h] to Meters[e]	–	50 m/s[i] to 150 m/s[g]	<1 kPa[f] to >10 kPa[f]	120 °C[g] to 450 °C[h]	4 km[h] to 30 km[g]	Up to 0.8 km[h] or n/a (blast)
Low-energy detached surge (LEDS)						
Few cm[e] to 20 cm[i] [<4 cm[a], few cm[b]]	2 m[b] to 10 m[a,b] [8–10 m[a], 2–10 m[b]]	1 m/s[b] to 10 m/s[a] [<10 m/s[a], ~1 m/s[b]]	<0.2 kPa[a] to 2 kPa[e] [<0.2 kPa[a], <0.5 kPa[b]]	100 °C[b] to ~400 °C[e] [200–300 °C[a], 100–200 °C[b]]	2.5 km[e] to 13.5 km[a] [13.5 km[a], 8.5 km[b]]	40 m[i] to 450 m[b] [200 m[a], 450 m[b]]

-: Missing values could not be reasonably inferred from available literature or imagery.
[a] Merapi (2010), Charbonnier et al. (2013), Jenkins et al. (2013, 2016), Komorowski et al. (2013), this study.
[b] Fuego (2018), this study.
[c] Merapi (2006), Charbonnier and Gertisser (2008), Gertisser et al. (2012).
[d] Colima (2015), Macorps et al. (2018).
[e] Soufrière Hills (1997), Druitt et al. (2002), Loughlin et al. (2002b).
[f] Mount Pelée (1902), Gueugneau et al. (2020).
[g] Mt. St. Helens (1980), Rosenbaum and Waitt (1981), Baxter (1990).
[h] Unzen (1991), Ikeya and Ishikawa (1993).
[i] Merapi (1994), Abdurachman et al. (2000).

is difficult, especially if inferred from field and remote studies alone, although sophisticated numerical models that aim to recreate the physical processes underlying PDC generation and transport can offer some insight (e.g., Esposti Ongaro et al., 2020), as may controlled experiments (e.g., Mastrolorenzo et al., 2010).

The range of observed characteristics across different eruptions but within unconfined PDCs of the same type (Table 1) can be related to a few potential factors. The size of the magma batch and the volume of erupted material may affect PDC temperatures at their generation, leading ultimately to differences in source temperatures between eruptions, before PDCs become unconfined. The PDC generation mechanism appears to affect the temperature of ensuing PDCs: collapsing lava domes (e.g., Soufrière Hills 1997, Merapi 1994, 2006, 2010) are correlated with higher initial PDC temperatures than a sector collapse (e.g., Fuego 2018), and this appears to play a stronger role than distance from the volcano. For example, PDCs at the affected sites near Fuego appear to have been either similar or lower temperature despite being closer to the volcano (~8 km) than the sites at Merapi (~13 km). Finally, the path and transportation conditions can affect the temperature, dynamic pressure, mass load, and velocity as shown during the paroxysmal phase of the 5 November 2010 eruption at Merapi where the PDC was strongly deviated by a ridge then funnelled into a major topographic constriction that created a large-scale venturi effect. This in turn generated a drastic acceleration and expansion of the unconfined PDC outside the constriction which thus gained laterally-directed blast dynamics at a location off-centered and 3 km away from the initial source (Komorowski et al., 2013; Jenkins et al., 2013).

The velocity (and therefore the dynamic pressure) of PDCs seems to be strongly influenced by the cause of unconfinement. Based on recorded examples, PDCs unconfined from inception (e.g., directed blast at Mt. Pelée 1902) and those that simply outrun their valley-confined, parent flows (e.g., high-energy surges at Unzen 1991) seem capable of maintaining their high velocities (>60 m/s), while those caused by channel bends or constrictions (e.g., slow overspills and LEDS at Merapi 1994 and 2010) often decrease in velocity drastically soon after leaving the channel to the speeds inferred in this study (<10 m/s). Unconfined PDCs, despite their lower velocities, can maintain high mobility, flowing kilometres downstream after unconfinement (e.g., Merapi 2010, Fuego 2018) or even reforming confined flows when encountering a new channel (e.g., Soufrière Hills June 1997; Druitt et al., 2002). As a general rule, LEDS are the slowest-moving (a few m/s) and most dilute (<5 kg/m^3) of the unconfined PDCs, resulting in the lowest dynamic pressures (<0.5 kPa) and thus the least mechanical damage to buildings. LEDS deposits are typically no thicker than 20 cm, with satellite imagery and field visits following the Fuego and Merapi eruptions showing that most of their deposits were on the order of a few centimetres and had already been washed away within as little as a few weeks. The ease with which LEDS deposits can be eroded and washed away means that they are poorly preserved in the geological record. However, in all previous cases where LEDS have inundated still inhabited areas, they were hot enough to be deadly to their farthest extent.

LEDS are unique amongst the unconfined PDCs discussed here as they impart little mechanical impact and leave only very thin deposits but can still be fatal. A wide range of LEDS emplacement temperatures exists, with thermal impacts on plastics, vegetation and clothes suggesting relatively low temperatures of around 100–220 °C in San Miguel Los Lotes, Fuego, ~200–300 °C in Bronggang, Merapi, and >400 °C in Streatham, Soufrière Hills. In Bronggang, less than 10% of the 59 people affected by the LEDS survived. Media images show that some of the deaths in San Miguel Los Lotes, especially in the southern end of town less affected by dense flows, were the result of people being caught in LEDS. In both the Merapi 2010 and Fuego 2018 eruptions, LEDS deaths occurred due to severe burns and hot ash inhalation both inside and outside buildings, evidenced by bodies found in a pugilistic attitude, with clothing often intact. Flow overspills were responsible for many more deaths in the Fuego eruption than at Merapi; a complex combination of political, cultural, economic, and demographic factors, unrelated to PDC dynamics or geology, likely played an important role. San Miguel Los Lotes was significantly more populated than Bakalan and was not evacuated prior to the eruption, meaning that fatality in the northern part of the village highly affected by flows would have been near total. In Bakalan, there were only four or five casualties thanks to prior evacuation. Similarly, at La Reunión, loss of life was prevented by a full evacuation prior to the arrival of PDCs.

Fires following the inundation of PDC can cause more damage than the PDC itself, although with dense PDCs the evidence of damage can be buried. Widespread fire following the directed blast of Pelée 1902 incinerated the town of St. Pierre, leaving no evidence of the thermal impact of the PDC itself. In all recorded LEDS, localised fires were ignited and at Merapi, this could be attributed to embers (firebrands) carried within the LEDS (Jenkins et al., 2013). It is reasonable to infer that in situations with fewer firebrands present (e.g., fewer trees consumed in the surge path), the likelihood of building damage from LEDS may be lower. Building typology is also a factor affecting the level of damage sustained during LEDS, with timber buildings much more likely to be damaged in a LEDS-caused fire than masonry buildings. Considering these factors, fire damage resulting from LEDS is likely to be higher in dry areas and/or during dry seasons and in areas containing buildings made from more flammable material. Conversely, it is possible that the potential for building damage from LEDS could be diminished or discounted in arid unvegetated areas, where building types are less flammable, if flammable items are removed prior to inundation, and/or during the rainy season or in wet areas. However, the rapid inundation of multiple PDCs in a short amount of time (as at Bronggang) can act to dry out wet vegetation or other sources of fuel priming it for ignition.

By their nature, unconfined PDCs are difficult to forecast because they inundate areas beyond the topographic lows that are typically given priority in volcanic hazard planning. As numerical models become more sophisticated (e.g., Esposti Ongaro et al., 2008; Kelfoun et al., 2017; Lube et al., 2020; Gueugneau et al., 2021), they may be better able to recreate, and therefore forecast, the path and dynamics of unconfined PDCs. In the meantime, one approach in mitigation planning has been to apply a 'buffer' (e.g., Neri et al., 2015) around a PDC-prone channel to highlight threatened populations and infrastructure, with the aim of implementing long-term land-use or short-term proactive evacuation measures for communities close to topographic lows. The extent of this buffer is difficult to define, and is a function of the channel topography, PDC volume and local PDC mass flux/velocity as well as preceding events in the eruption sequence (e.g., the infilling by previous PDC deposits). For directed blasts, a buffer is clearly not appropriate because of their wide-reaching and topography-mantling nature, in these cases an energy cone model that defines distance from the summit may be useful. For those high-energy surges that are not unconfined from origin, e.g., Unzen 1991, this type of model is less useful as it is unable to identify locations of surge detachment. For overspill PDCs, we found they reach a maximum lateral distance of 800 m (Table 1) from the flowpath channel. However, we recognise that buffer extents are likely to be unique to the specific eruptions and require consideration of the topography, channel path and likely eruptive style. Reliance on geological deposits for defining buffers and potentially hazardous areas must be cognisant of the thinner deposits that reflect unconfined PDCs that cannot be preserved but are still deadly. Human modification of the landscape must also be accounted for, as data from the Merapi 2010 eruption reveals that in some cases river channel engineering structures (e.g., sabo dam, valley walls, paved valley sides) can modify the dynamics of primary PDCs and favour the generation of damaging and especially lethal LEDS even near the distal PDC flow terminus.

Volcanic hazard and risk assessment relies upon empirical data from past eruptions and their impacts. However, we are often limited in the amount of data that can be collected shortly after an event, while deposits and impacts are preserved, because of safety and access limitations. This preservation is what makes extracting quantitative data

about a PDC from its deposit and impact such a valuable effort despite its difficulty. Despite uncertainties caused by the fact that this information is collected after the event, the variability in amount and detail of data obtainable, the extrapolated rather than observed nature of this information, and the difficulty researchers face when collecting this data as shortly as possible after a disaster with casualties and widespread damage, these techniques are paramount to improve the understanding of past events and to refine the parametrization of complex physical models that allow the elaboration of a range of deterministic as well as probabilistic scenarios of potential future crises.

In this study, we have used lessons learned from remote and ground surveys of PDC dynamics following the Merapi 2010 eruption to provide a similar assessment for Fuego 2018. Remote assessment at Fuego using satellite imagery and media images to supplement a field study allowed for many similar determinations of PDC dynamics and resultant impacts as at Merapi. In both cases, through imagery or direct observation, building damage, extent of casualties, condition of vegetation, and state of materials like plastics and fabrics could be extrapolated into velocities, concentrations, dynamic pressures, temperatures, and the height of the associated PDCs. Personal familiarity with the affected area as well as presence on site allowed for more precise damage evaluation of buildings, as well as a more thorough record of geo-referenced photos than could be obtained through media images. Another vital piece of information provided by field studies is geological information. Detailed stratigraphic study and deposit analysis at Merapi was obtained over multiple field visits and these data, when combined with the impact assessment, were valuable for making inferences about PDC processes, whereas discussion of PDC dynamics at Fuego relied upon remote imagery and information from one field study, for which the focus was on deposits and not impacts. As shown at Merapi and Fuego, depending on the circumstances of the study, both remote and on-the-ground analysis serve a vital role in inferring the PDC characteristics that inform hazard models, mitigation, and risk assessment.

Author statement

SFJ devised the study. SFJ, SJC, PJB, and JCK performed fieldwork and/or in-person damage assessment. GAL and SFJ curated and compiled data. GAL and SFJ performed remote hazard assessment. GAL and SFJ wrote the first draft. GAL, SFJ, SJC, PJB, and JCK reviewed and edited the manuscript.

Declaration of Competing Interest

The authors declare that they have no known competing financial interests or personal relationships that could have appeared to influence the work reported in this paper.

Acknowledgements

The authors are grateful to Eric Breard and an anonymous reviewer for highly constructive feedback which resulted in improvements to the manuscript. The authors thank JVGR editor James Gardner for his handling of our manuscript. GAL and SFJ acknowledge funding from AXA and Singapore National Research Foundation (NRF2018NRF-NSFC003ES-010). This research was supported by the Earth Observatory of Singapore via its funding from the National Research Foundation Singapore and the Singapore Ministry of Education under the Research Centres of Excellence initiative. This work comprises EOS contribution number 371. SFJ, PJB and JCK are grateful for funding from the European Union (MIAVITA) and Agence Nationale de la Recherche (CASAVA). PJB acknowledges funding from the Pan American Health Organisation. SJC would like to acknowledge NSF RAPID grant #1841852 and colleagues from the Fuego 2018 eruption crisis response team. The authors would like to acknowledge CVGHM, BPPTK, and INSIVUMEH for their cooperation and responses to the Merapi 2010 and Fuego 2018 eruptions. We are grateful to Nguyen Thi Nam Phuong for creating of the schematic portion of Fig. 6. We would like to acknowledge an anonymous photographer for providing the non-credited photos used in Fig. 9. We are grateful to Maxar Technologies for providing the statellite imagery use in Fig. 9c through their Open Data Program. We are grateful to Chai Min Wei who, in the weeks following the June 2018 Fuego eruption, collated many of the available media images.

References

Abdurachman, E.K., Bourdier, J.-L., Voight, B., 2000. Nuées ardentes of 22 November 1994 at Merapi volcano, Java, Indonesia. J. Volcanol. Geotherm. Res. 100, 345–361. https://doi.org/10.1016/S0377-0273(00)00144-X.

Albino, F., Biggs, J., Escobar-Wolf, R., Naismith, A., Watson, M., Phillips, J.C., Chigna Marroquin, G.A., 2020. Using TanDEM-X to measure pyroclastic flow source location, thickness and volume: Application to the 3rd June 2018 eruption of Fuego volcano, Guatemala. J. Volcanol. Geotherm. Res. 406, 107063. https://doi.org/10.1016/j.jvolgeores.2020.107063.

Anderson, T., Flett, J.S., 1902. Preliminary report on the recent eruption of the Soufrière in St. Vincent, and of a visit to Mont Pelée, in Martinique. Proc. R. Soc. Lond. 70, 423–445. https://doi.org/10.1098/rspl.1902.0042.

Barcík, Š., Gašparík, M., Razumov, E.Y., 2014. Effect of temperature on the color changes of wood during thermal modification. Cellul. Chem. Technol. 49, 789–798.

Baxter, P.J., 1990. Medical effects of volcanic eruptions: I. Main causes of death and injury. Bull. Volcanol. 52, 532–544. https://doi.org/10.1007/BF00301534.

Baxter, P.J., Horwell, C.J., 2015. Impacts of Eruptions on Human Health. The Encyclopedia of Volcanoes. Elsevier, pp. 1035–1047 https://doi.org/10.1016/B978-0-12-385938-9.00060-2.

Baxter, P.J., Boyle, R., Cole, P., Neri, A., Spence, R., Zuccaro, G., 2005. The impacts of pyroclastic surges on buildings at the eruption of the Soufrière Hills volcano, Montserrat. Bull. Volcanol. 67, 292–313. https://doi.org/10.1007/s00445-004-0365-7.

Baxter, P.J., Jenkins, S., Seswandhana, R., Komorowski, J.-C., Dunn, K., Purser, D., Voight, B., Shelley, I., 2017. Human survival in volcanic eruptions: thermal injuries in pyroclastic surges, their causes, prognosis and emergency management. Burns 43, 1051–1069. https://doi.org/10.1016/j.burns.2017.01.025.

Belousov, A., Voight, B., Belousova, M., 2007. Directed blasts and blast-generated pyroclastic density currents: a comparison of the Bezymianny 1956, Mount St Helens 1980, and Soufrière Hills, Montserrat 1997 eruptions and deposits. Bull. Volcanol. 69, 701. https://doi.org/10.1007/s00445-006-0109-y.

Belousov, A., Belousova, M., Hoblitt, R., Patia, H., 2020. The 1951 eruption of Mount Lamington, Papua New Guinea: devastating directed blast triggered by small-scale edifice failure. J. Volcanol. Geotherm. Res. 401, 106947. https://doi.org/10.1016/j.jvolgeores.2020.106947.

Benage, M.C., Dufek, J., Mothes, P.A., 2016. Quantifying entrainment in pyroclastic density currents from the Tungurahua eruption, Ecuador: integrating field proxies with numerical simulations. Geophys. Res. Lett. 43, 6932–6941. https://doi.org/10.1002/2016GL069527.

Bogoyavlenskaya, G.E., Braitseva, O.A., Melekestsev, I.V., Kiriyanov, V.Yu., Dan Miller, C., 1985. Catastrophic eruptions of the directed-blast type at Mount St. Helens, bezymianny and Shiveluch volcanoes. J. Geodyn. 3, 189–218. https://doi.org/10.1016/0264-3707(85)90035-3.

Bourdier, J.L., Boudon, G., Gourgaud, A., 1989. Stratigraphy of the 1902 and 1929 nuée-ardente deposits, Mt. Pelée, Martinique. J. Volcanol. Geotherm. Res. 38, 77–96. https://doi.org/10.1016/0377-0273(89)90031-0.

Breard, E., Dufek, J., Roche, O., 2019. Continuum modelling of pressure-balanced and fluidized granular flows in 2D: comparison with glass bead experiments and implications for concentrated pyroclastic currents. J. Geophys. Res. Solid Earth 124. https://doi.org/10.1029/2018JB016874.

Breard, E.C.P., 2016. Dynamics of Pyroclastic Density Current. Massey University, Palmerston North, New Zealand.

Breard, E.C.P., Lube, G., 2017. Inside pyroclastic density currents – Uncovering the enigmatic flow structure and transport behaviour in large-scale experiments. Earth Planet. Sci. Lett. 458, 22–36. https://doi.org/10.1016/j.epsl.2016.10.016.

Brosch, E., Lube, G., 2020. Spatiotemporal sediment transport and deposition processes in experimental dilute pyroclastic density currents. J. Volcanol. Geotherm. Res. 401, 106946. https://doi.org/10.1016/j.jvolgeores.2020.106946.

Brown, R.J., Andrews, G.D.M., 2015. Chapter 36 - Deposits of pyroclastic density currents. In: Sigurdsson, H. (Ed.), The Encyclopedia of Volcanoes (Second Edition). Academic Press, Amsterdam, pp. 631–648 https://doi.org/10.1016/B978-0-12-385938-9.00036-5.

Brown, S.K., Jenkins, S.F., Sparks, R.S.J., Odbert, H., Auker, M.R., 2017. Volcanic fatalities database: analysis of volcanic threat with distance and victim classification. J. Appl. Volcanol. 6, 15. https://doi.org/10.1186/s13617-017-0067-4.

BSI, B., 1996. 6399–1, Loading for buildings, in: Code of Practice for Dead and Imposed Loads. BSI, London, UK.

Bursik, M.I., Kurbatov, A.V., Sheridan, M.F., Woods, A.W., 1998. Transport and deposition in the May 18, 1980, Mount St. Helens blast flow. Geology 26, 155–158. https://doi.org/10.1130/0091-7613(1998)026<0155:TADITM>2.3.CO;2.

Charbonnier, S., Gertisser, R., 2012. Evaluation of geophysical mass flow models using the 2006 block-and-ash flows of Merapi Volcano, Java, Indonesia: Towards a short-term hazard assessment tool. J. Volcanol. Geother. Res. 231–232, 87–108. https://doi.org/10.1016/j.jvolgeores.2012.02.015.

Charbonnier, S.J., Gertisser, R., 2008. Field observations and surface characteristics of pristine block-and-ash flow deposits from the 2006 eruption of Merapi Volcano, Java, Indonesia. J. Volcanol. Geother. Res. Volcanic Flows Falls 177, 971–982. https://doi.org/10.1016/j.jvolgeores.2008.07.008.

Charbonnier, S.J., Gertisser, R., 2011. Deposit architecture and dynamics of the 2006 block-and-ash flows of Merapi Volcano, Java, Indonesia. Sedimentology 58, 1573–1612. https://doi.org/10.1111/j.1365-3091.2011.01226.x.

Charbonnier, S.J., Germa, A., Connor, C.B., Gertisser, R., Preece, K., Komorowski, J.-C., Lavigne, F., Dixon, T., Connor, L., 2013. Evaluation of the impact of the 2010 pyroclastic density currents at Merapi volcano from high-resolution satellite imagery, field investigations and numerical simulations. J. Volcanol. Geotherm. Res. 261, 295–315. https://doi.org/10.1016/j.jvolgeores.2012.12.021.

Clarke, A.B., Voight, B., 2000. Pyroclastic current dynamic pressure from aerodynamics of tree or pole blow-down. J. Volcanol. Geotherm. Res. 100, 395–412. https://doi.org/10.1016/S0377-0273(00)00148-7.

Cole, P.D., Calder, E.S., Sparks, R.S.J., Clarke, A.B., Druitt, T.H., Young, S.R., Herd, R.A., Harford, C.L., Norton, G.E., 2002. Deposits from dome-collapse and fountain-collapse pyroclastic flows at Soufrière Hills Volcano, Montserrat. Geol. Soc. Lond. Mem. 21, 231–262. https://doi.org/10.1144/GSL.MEM.2002.021.01.11.

Cole, P.D., Neri, A., Baxter, P.J., 2015. Chapter 54 - Hazards from pyroclastic density currents. In: Sigurdsson, H. (Ed.), The Encyclopedia of Volcanoes (Second Edition). Academic Press, Amsterdam, pp. 943–956 https://doi.org/10.1016/B978-0-12-385938-9.00054-7.

Cooper, M.J.M., 2018. The Mt. Unzen Disaster: A Terrible Learning Experience. In: Chakraborty, A., Mokudai, K., Cooper, M., Watanabe, M., Chakraborty, S. (Eds.), Natural Heritage of Japan, Geoheritage. Geoparks and Geotourism. Springer International Publishing, Cham, pp. 131–142 https://doi.org/10.1007/978-3-319-61896-8_12.

Cronin, S.J., Lube, G., Dayudi, D.S., Sumarti, S., Subrandiyo, S., Surono, 2013. Insights into the October–November 2010 Gunung Merapi eruption (Central Java, Indonesia) from the stratigraphy, volume and characteristics of its pyroclastic deposits. J. Volcanol. Geother. Res. Merapi eruption 261, 244–259. https://doi.org/10.1016/j.jvolgeores.2013.01.005.

Dellino, P., Büttner, R., Dioguardi, F., Doronzo, D.M., La Volpe, L., Mele, D., Sonder, I., Sulpizio, R., Zimanowski, B., 2010. Experimental evidence links volcanic particle characteristics to pyroclastic flow hazard. Earth Planet. Sci. Lett. 295, 314–320. https://doi.org/10.1016/j.epsl.2010.04.022.

Druitt, T.H., Calder, E.S., Cole, P.D., Hoblitt, R.P., Loughlin, S.C., Norton, G.E., Ritchie, L.J., Sparks, R.S.J., Voight, B., 2002. Small-volume, highly mobile pyroclastic flows formed by rapid sedimentation from pyroclastic surges at Soufrière Hills Volcano, Montserrat: an important volcanic hazard. Geol. Soc. Lond. Mem. 21, 263–279. https://doi.org/10.1144/GSL.MEM.2002.021.01.12.

Esposti Ongaro, T., Clarke, A.B., Neri, A., Voight, B., Widiwijayanti, C., 2008. Fluid dynamics of the 1997 Boxing Day volcanic blast on Montserrat, West Indies. J. Geophys. Res. Solid Earth 113. https://doi.org/10.1029/2006JB004898.

Esposti Ongaro, T., Widiwijayanti, C., Clarke, A.B., Voight, B., Neri, A., 2011. Multiphase-flow numerical modeling of the 18 May 1980 lateral blast at Mount St. Helens, USA. Geology 39, 535–538. https://doi.org/10.1130/G31865.1.

Esposti Ongaro, T., Clarke, A.B., Voight, B., Neri, A., Widiwijayanti, C., 2012. Multiphase flow dynamics of pyroclastic density currents during the May 18, 1980 lateral blast of Mount St. Helens. J. Geophys. Res. Solid Earth, 117 https://doi.org/10.1029/2011JB009081.

Esposti Ongaro, T., Komorowski, J.-C., Legendre, Y., Neri, A., 2020. Modelling pyroclastic density currents from a subplinian eruption at La Soufrière de Guadeloupe (West Indies, France). Bull. Volcanol. 82, 76. https://doi.org/10.1007/s00445-020-01411-6.

Ferrés, D., Escobar Wolf, R., 2018. Informe técnico: Volcan de Fuego (Technical Report). Cooperación Espanola.

Fisher, R.V., 1995. Decoupling of pyroclastic currents: hazards assessments. J. Volcanol. Geotherm. Res. 66, 257–263. https://doi.org/10.1016/0377-0273(94)00075-R.

Flynn, I.T.W., Ramsey, M.S., 2020. Pyroclastic Density current hazard assessment and modeling uncertainties for Fuego Volcano, Guatemala. Remote Sens. 12, 2790. https://doi.org/10.3390/rs12172790.

Fujii, T., Nakada, S., 1999. The 15 September 1991 Pyroclastic Flows at Unzen Volcano ŽJapan/: A Flow Model for Associated Ash-cloud Surges 14.

Gertisser, R., Cassidy, N.J., Charbonnier, S.J., Nuzzo, L., Preece, K., 2012. Overbank block-and-ash flow deposits and the impact of valley-derived, unconfined flows on populated areas at Merapi volcano, Java, Indonesia. Nat. Hazards 60, 623–648. https://doi.org/10.1007/s11069-011-0044-x.

Gueugneau, V., Kelfoun, K., Charbonnier, S., Germa, A., Carazzo, G., 2020. Dynamics and Impacts of the May 8th, 1902 pyroclastic current at Mount Pelée (Martinique): new insights from numerical modeling. Front. Earth Sci. 8. https://doi.org/10.3389/feart.2020.00279.

Gueugneau, V., Charbonnier, S., Esposti Ongaro, T., de' Michieli Vitturi, M., Peruzzetto, M., Mangeney, A., Bouchut, F., Patra, A., Kelfoun, K., 2021. Synthetic benchmarking of concentrated pyroclastic current models. Bull. Volcanol. 83, 1–32. https://doi.org/10.1007/s00445-021-01491-y.

Hovey, E.O., 1904. The 1902–1903 Eruptions of Mont Pelé, Martinique and the Soufrière. St. Vincent, Brothers Hollinek.

Ikeya, H., Ishikawa, Y., 1993. Characteristics of Pyroclastic Flows and Debris Flows Accompanying the Mt Unzen-Fugendake Eruption. IAHS Press.

Jenkins, S., Komorowski, J.-C., Baxter, P.J., Spence, R., Picquout, A., Lavigne, F., Surono, 2013. The Merapi 2010 eruption: an interdisciplinary impact assessment methodology for studying pyroclastic density current dynamics. J. Volcanol. Geotherm. Res. 261, 316–329. https://doi.org/10.1016/j.jvolgeores.2013.02.012.

Jenkins, S.F., Komorowski, J.-C., Baxter, P.J., Charbonnier, S.J., Cholik, N., Surono, 2016. The devastating impact of the 2010 Eruption of Merapi Volcano, Indonesia. In: Duarte, J.C., Schellart, W.P. (Eds.), Geophysical Monograph Series. John Wiley & Sons, Inc., Hoboken, NJ, USA, pp. 259–269 https://doi.org/10.1002/9781119054146.ch12.

Kelfoun, K., Gueugneau, V., Komorowski, J.-C., Aisyah, N., Cholik, N., Merciecca, C., 2017. Simulation of block-and-ash flows and ash-cloud surges of the 2010 eruption of Merapi volcano with a two-layer model. J. Geophys. Res. Solid Earth 122, 4277–4292. https://doi.org/10.1002/2017JB013981.

Komorowski, J.-C., Jenkins, S., Baxter, P.J., Picquout, A., Lavigne, F., Charbonnier, S., Gertisser, R., Preece, K., Cholik, N., Budi-Santoso, A., Surono, 2013. Paroxysmal dome explosion during the Merapi 2010 eruption: Processes and facies relationships of associated high-energy pyroclastic density currents. J. Volcanol. Geotherm. Res. 261, 260–294. https://doi.org/10.1016/j.jvolgeores.2013.01.007.

Lacroix, A., 1904. La Montagne Pelee et ses eruptions. Masson.

Lavigne, F., Komorowski, J.C., Jenkins, S., Baxter, P., Vidal, C., Mei, E.T.W., Picquout, A., Grancher, D., Brunstein, D., 2011. Satellite remote-sensing and field analysis of casualties and damage caused by the 2010 eruption of Merapi volcano Indonesia. Remote Sensing, Natural hazards and Environmental Change, 28–29 July 2011. Centre for Remote Sensing and Processing (CRISP) NUS, Singapore.

Lipman, P.W., Mullineaux, D.R., 1982. The 1980 Eruptions of Mount St. U.S. Department of the Interior, U.S. Geological Survey, Helens, Washington.

Loughlin, S.C., Baxter, P.J., Aspinall, W.P., Darroux, B., Harford, C.L., Miller, A.D., 2002a. Eyewitness accounts of the 25 June 1997 pyroclastic flows and surges at Soufrière Hills Volcano, Montserrat, and implications for disaster mitigation. Geol. Soc. Lond. Mem. 21, 211–230. https://doi.org/10.1144/GSL.MEM.2002.021.01.10.

Loughlin, S.C., Calder, E.S., Clarke, A., Cole, P.D., Luckett, R., Mangan, M.T., Pyle, D.M., Sparks, R.S.J., Voight, B., Watts, R.B., 2002b. Pyroclastic flows and surges generated by the 25 June 1997 dome collapse, Soufrière Hills Volcano, Montserrat. Geol. Soc. Lond. Mem. 21, 191–209. https://doi.org/10.1144/GSL.MEM.2002.021.01.09.

Lube, G., Cronin, S.J., Thouret, J.-C., Surono, 2011. Kinematic characteristics of pyroclastic density currents at Merapi and controls on their avulsion from natural and engineered channels. GSA Bull. 123, 1127–1140. https://doi.org/10.1130/B30244.1.

Lube, G., Breard, E.C.P., Cronin, S.J., Jones, J., 2015. Synthesizing large-scale pyroclastic flows: Experimental design, scaling, and first results from PELE. J. Geophys. Res. Solid Earth 120, 1487–1502. https://doi.org/10.1002/2014JB011666.

Lube, G., Breard, E.C.P., Esposti-Ongaro, T., Dufek, J., Brand, B., 2020. Multiphase flow behaviour and hazard prediction of pyroclastic density currents. Nat. Rev. Earth Environ. 1, 348–365. https://doi.org/10.1038/s43017-020-0064-8.

Macorps, E., Charbonnier, S.J., Varley, N.R., Capra, L., Atlas, Z., Cabré, J., 2018. Stratigraphy, sedimentology and inferred flow dynamics from the July 2015 block-and-ash flow deposits at Volcán de Colima, Mexico. J. Volcanol. Geotherm. Res. 349, 99–116. https://doi.org/10.1016/j.jvolgeores.2017.09.025.

Mastrolorenzo, G., Petrone, P., Pappalardo, L., Guarino, F.M., 2010. Lethal Thermal Impact at Periphery of Pyroclastic Surges: Evidences at Pompeii. PLoS One 5, e11127. https://doi.org/10.1371/journal.pone.0011127.

Miyahara, T., Endo, K., Tohno, I., Chiba, T., Iso, N., Senda, K., Shinkawa, K., Yasui, M., Komori, J., Ohno, M., 1992. Eruptive products of the 1991 Unzen-Hugendake eruption (1). Proc. Inst. Nat. Sci. 27, 71–80.

Nairn, I.A., Self, S., 1978. Explosive eruptions and pyroclastic avalanches from Ngauruhoe in February 1975. J. Volcanol. Geotherm. Res. 3, 39–60. https://doi.org/10.1016/0377-0273(78)90003-3.

Naismith, A., Armijos, M.T., Escobar, E.A.B., Chigna, W., Watson, I.M., 2020. Fireside tales: understanding experiences of previous eruptions and factors influencing the decision to evacuate from activity of Volcán de Fuego. Volcanica 3, 205–226. https://doi.org/10.30909/vol.03.02.205226.

Naismith, A.K., Matthew Watson, I., Escobar-Wolf, R., Chigna, G., Thomas, H., Coppola, D., Chun, C., 2019. Eruption frequency patterns through time for the current (1999–2018) activity cycle at Volcán de Fuego derived from remote sensing data: Evidence for an accelerating cycle of explosive paroxysms and potential implications of eruptive activity. J. Volcanol. Geotherm. Res. 371, 206–219. https://doi.org/10.1016/j.jvolgeores.2019.01.001.

Nakada, S., Fujii, T., 1993. Preliminary report on the activity at Unzen Volcano (Japan), November 1990-November 1991: Dacite lava domes and pyroclastic flows. J. Volcanol. Geotherm. Res. 54, 319–333. https://doi.org/10.1016/0377-0273(93)90070-8.

Neri, A., Ongaro, T.E., Macedonio, G., Gidaspow, D., 2003. Multiparticle simulation of collapsing volcanic columns and pyroclastic flow. J. Geophys. Res. Solid Earth 108. https://doi.org/10.1029/2001JB000508.

Neri, A., Esposti Ongaro, T., Voight, B., Widiwijayanti, C., 2015. Pyroclastic density current hazards and risk. Volcanic Hazards, Risks and Disasters, pp. 109–140 https://doi.org/10.1016/B978-0-12-396453-3.00005-8.

Newhall, C.G., Bronto, S., Alloway, B., Banks, N.G., Bahar, I., del Marmol, M.A., Hadisantono, R.D., Holcomb, R.T., McGeehin, J., Miksic, J.N., Rubin, M., Sayudi, S.D., Sukhyar, R., Andreastuti, S., Tilling, R.I., Torley, R., Trimble, D., Wirakusumah, A.D., 2000. 10,000Years of explosive eruptions of Merapi Volcano, Central Java: archaeological and modern implications. J. Volcanol. Geotherm. Res. 100, 9–50. https://doi.org/10.1016/S0377-0273(00)00132-3.

Ogburn, S.E., Calder, E.S., Cole, P.D., Stinton, A.J., 2014. Chapter 10 The effect of topography on ash-cloud surge generation and propagation. Geol. Soc. Lond. Mem. 39, 179–194. https://doi.org/10.1144/M39.10.

Pallister, J.S., Schneider, D.J., Griswold, J.P., Keeler, R.H., Burton, W.C., Noyles, C., Newhall, C.G., Ratdomopurbo, A., 2013. Merapi 2010 eruption—Chronology and extrusion rates monitored with satellite radar and used in eruption forecasting. J. Volcanol. Geother. Res. Merapi eruption 261, 144–152. https://doi.org/10.1016/j.jvolgeores.2012.07.012.

Pardini, F., Queißer, M., Naismith, A., Watson, I.M., Clarisse, L., Burton, M.R., 2019. Initial constraints on triggering mechanisms of the eruption of Fuego volcano (Guatemala) from 3 June 2018 using IASI satellite data. J. Volcanol. Geotherm. Res. 376, 54–61. https://doi.org/10.1016/j.jvolgeores.2019.03.014.

Pensa, A., Capra, L., Giordano, G., Corrado, S., 2018. Emplacement temperature estimation of the 2015 dome collapse of Volcán de Colima as key proxy for flow dynamics of confined and unconfined pyroclastic density currents. J. Volcanol. Geotherm. Res. 357, 321–338. https://doi.org/10.1016/j.jvolgeores.2018.05.010.

Pensa, A., Capra, L., Giordano, G., 2019. Ash clouds temperature estimation. Implication on dilute and concentrated PDCs coupling and topography confinement. Sci. Rep. 9, 5657. https://doi.org/10.1038/s41598-019-42035-x.

Pittari, A., Cas, R.A.F., Monaghan, J.J., Martí, J., 2006. Instantaneous dynamic pressure effects on the behaviour of lithic boulders in pyroclastic flows: the Abrigo Ignimbrite, Tenerife, Canary Islands. Bull. Volcanol. 69, 265–279. https://doi.org/10.1007/s00445-006-0072-7.

Rosenbaum, J.G., Waitt, R.B., 1981. The 1980 eruptions of Mount St Helens, Washington. Summary of eye witness accounts of the May 18 eruption. In: Lipman, P.W., Mullineaux, D.R. (Eds.), The 1980 Eruptions of Mount St Helens, Geol Surv Prof Pap. US Govt Printing Office, Washington, DC, pp. 53–67.

Rosi, M., Principe, C., Vecci, R., 1993. The 1631 Vesuvius eruption. A reconstruction based on historical and stratigraphical data. J. Volcanol. Geother. Res., Mount Vesuvius 58, 151–182. https://doi.org/10.1016/0377-0273(93)90106-2.

Shimizu, H.A., Koyaguchi, T., Suzuki, Y.J., 2019. The run-out distance of large-scale pyroclastic density currents: a two-layer depth-averaged model. J. Volcanol. Geotherm. Res. 381, 168–184. https://doi.org/10.1016/j.jvolgeores.2019.03.013.

Sparks, R., Barclay, J., Calder, E., Herd, R., Komorowski, J.-C., Luckett, R., Norton, G., Ritchie, L., Voight, B., Woods, A., 2002. Generation of a debris avalanche and violent pyroclastic density current on 26 December (Boxing Day) 1997 at Soufriere Hills Volcano, Montserrat. Geol. Soc. Lond. Mem. 21, 409–434. https://doi.org/10.1144/GSL.MEM.2002.021.01.18.

Sulpizio, R., Dellino, P., 2008. Chapter 2 sedimentology, depositional mechanisms and pulsating behaviour of pyroclastic density currents. In: Gottsmann, J., Martí, J. (Eds.), Developments in Volcanology, Caldera Volcanism: Analysis, Modelling and Response. Elsevier, pp. 57–96 https://doi.org/10.1016/S1871-644X(07)00002-2.

Surono, Jousset P., Pallister, J., Boichu, M., Buongiorno, M.F., Budisantoso, A., Costa, F., Andreastuti, S., Prata, F., Schneider, D., Clarisse, L., Humaida, H., Sumarti, S., Bignami, C., Griswold, J., Carn, S., Oppenheimer, C., Lavigne, F., 2012. The 2010 explosive eruption of Java's Merapi volcano—A '100-year' event. J. Volcanol. Geotherm. Res. 241–242, 121–135. https://doi.org/10.1016/j.jvolgeores.2012.06.018.

Trolese, M., Giordano, G., Komorowski, J.-C., Jenkins, S.F., Baxter, P.J., Cholik, N., Raditya, P., Corrado, S., 2018. Very rapid cooling of the energetic pyroclastic density currents associated with the 5 November 2010 Merapi eruption (Indonesia). J. Volcanol. Geotherm. Res. 358, 1–12. https://doi.org/10.1016/j.jvolgeores.2018.06.004.

Valentine, G.A., 1998. Damage to structures by pyroclastic flows and surges, inferred from nuclear weapons effects. J. Volcanol. Geotherm. Res. 87, 117–140.

Valentine, G.A., Wohletz, K.H., 1989. Numerical models of Plinian eruption columns and pyroclastic flows. J. Geophys. Res. Solid Earth 94, 1867–1887. https://doi.org/10.1029/JB094iB02p01867.

Varner, L.A., Charbonnier, S.J., Escobar-Wolf, R.P., Rodriguez, L.A., Chigna, G., Chun, C., Gonzalez, D., Juarez, F., Merida, R., Calder, E., Germa, A., 2019. Unravelling the Dynamics and Hazards of the June 3rd, 2018 Pyroclastic Currents at Fuego volcano (Guatemala): A Multi-Parameter Approach 2019, V13E-0229.

Voight, B., Davis, M.J., 2000. Emplacement temperatures of the November 22, 1994 nuée ardente deposits, Merapi Volcano, Java. J. Volcanol. Geotherm. Res. 100, 371–377. https://doi.org/10.1016/S0377-0273(00)00146-3.

Voight, B., Constantine, E.K., Siswowidjoyo, S., Torley, R., 2000. Historical eruptions of Merapi Volcano, Central Java, Indonesia, 1768–1998. J. Volcanol. Geotherm. Res. 100, 69–138. https://doi.org/10.1016/S0377-0273(00)00134-7.

White, N., 2018. Shocking Satellite Photos Show Entire Towns Obliterated after Guatemala's "Volcano of Fire" Buried them in Tons of Ash that Crushed Hundreds of Homes and burned 300 People Alive. Mail Online.

Wibowo, H.E., Purnama Edra, A., Harijoko, A., Anggara, F., 2018. Emplacement temperature of the overbank and dilute-detached pyroclastic density currents of Merapi 5 November 2010 events using reflectance analysis of associated charcoal. J. Appl. Geol. 3, 41. https://doi.org/10.22146/jag.42445.

World Bank, 2018. Volcán de Fuego Guatemala Eruption Global Rapid Post Disaster Damage Estimation Grade Report (Global Rapid Post Disaster Damage Estimation (GRADE) Report No. AUS000903)..

Yamamoto, T., Takarada, S., Suto, S., 1993. Pyroclastic flows from the 1991 eruption of Unzen volcano, Japan. Bull. Volcanol. 55, 166–175. https://doi.org/10.1007/BF00301514.